DIELECTRICS AND ION IMPLANTATION STUDIES

by

Chun Bun KWOK

A thesis
presented to the University of Manitoba
in fulfillment of the
thesis requirement for the degree of
Master of Science
in
Department of Physics

Winnipeg, Manitoba

ISBN 0-315-76621-2

DIELECTRICS AND ION IMPLANTATION STUDIES

BY

CHUN BUN KWOK

A thesis submitted to the Faculty of Graduate Studies of
the University of Manitoba in partial fulfillment of the requirements
of the degree of

MASTER OF SCIENCE

I hereby declare that I am the sole author of this thesis.

I authorize the University of Manitoba to lend this thesis to other institutions or individuals for the purpose of scholarly research.

KWOK Chun Bun

I further authorize the University of Manitoba to reproduce this thesis by photocopying or by other means, in total or in part, at the request of other institutions or individuals for the purpose of scholarly research.

KWOK Chun Bun

Table of Contents

Title page	i
Declaration	ii
Sign out page	iii
Table of contents	iv
List of Figures	vi
Abstract	xii
Acknowledgements	xiv
Chapter 1 : INTRODUCTION	1
1.1 : H^+:H_2^+ Implantation Study of Dielectric	1
1.2 : H^+:H_2^+ Implantation Study of a-Si:H Thin Film	3
1.3 : A New Technique of Electrical Contact Fabrication	4
1.4 : Plasma Interaction and Ion Implantation of a Refractory Material	5
Chapter 2 : THE NARODNY ION ACCELERATOR AND THE SURFACE RAMAN FACILITY	7
2.1 : The Narodny Ion Accelerator	7
2.2 : The Surface Raman Scattering Facility	9
Chapter 3 : EXPERIMENTAL DETAILS	11
3.1 : H^+:H_2^+ Implantation Study of Dielectrics	11
3.2 : H^+:H_2^+ Implantation Study of a-Si:H Thin Film	16
3.3 : A New Technique for Metal Contact Fibraction	22

3.4 : Plasma Interaction and Ion Implantation of Refractory Materials 25

Chapter 4 : OBSERVATIONS AND RESULTS 28

4.1 : H^+:H_2^+ Implantation Study of Dielectrics 28

4.2 H^+:H_2^+ Implantation Study of a-Si:H Thin Film 39

4.3 : A New Technique for Metal Contact Fibraction 61

4.4 : Plasma Interaction and Ion Implantation of Refractory Materials 61

Chapter 5 : CONCLUSIONS 71

5.1 : Conclusions and Suggestions for Future Research on Implantation Study of Dielectrics 71

5.1.a : Conclusions 71

5.1.b : Suggestions for Future Research 72

5.2 : Conclusions for H^+:H_2^+ Implantation Study of a-Si:H Thin Film 74

5.3 : Conclusions of Plasma Interaction and Ion Implantation 75

APPENDIX A : List of Publications for Author 78

REFERENCES 80

List of Figures

Figure 2.1 :	Schematic of the Narodny Ion Accelerator	8
Figure 2.2 :	Surface Raman Light Scattering Facility	10
Figure 3.1a :	Four-Point Probe System Set-up	12
Figure 3.1b :	Deposited Electrodes Method	13
Figure 3.2 :	High Vacuum Deposition System	15
Figure 3.3 :	Bulk Thermal Conductivity Measurement Lay-out	17
Figure 3.4a :	Scanning Electron Micrograph of a-Si:H film 2000 x, shows island like features which extend all the way to the other side of the film, resulting in columnar morphology	18
Figure 3.4b :	Columnar profile of the a-Si:H film: Grain boundaries intersecting the growing surface modify the surface profile of the film. At the intersection of the grain boundary and surface a grove with an opening angle ϕ is formed where σ_{gb} and σ_s are the grain boundaries and the surface energy densities respectively	19
Figure 3.5 :	Typical X-ray diffraction pattern of an amorphous films employed in this study (Cu 40/20)	21

Figure 3.6 :	Schematic representation of the target mounting assembly	24
Figure 3.7 :	Experimental arrangement for PIXE analysis	26
Figure 4.1a :	Raman spectrum of H_2^+ unimplanted Dielectric 'ISP'	29
Figure 4.1b :	Raman spectrum of H_2^+ implanted dielectric 'ISP', part I	30
Figure 4.1b :	Raman spectrum of H_2^+ implanted dielectric 'ISP', part II	31
Figure 4.2 :	Typical voltage vs. surface current for H_2^+ implanted dielectric 'ISP'	33
Figure 4.3 :	Characteristic bulk thermal breakdown at constant applied field	35
Figure 4.4 :	Temperature vs. time variation of Figure 4.3	36
Figure 4.5 :	Breakdown prevention from the Pre-Breakdown-Region at constant applied voltage	38
Figure 4.6a :	Pre-Breakdown-Region signature comparison using the FFT Procedure (Phase shift comparison)	40
Figure 4.6b :	Pre-Breakdown-Region signature comparison using the FFT Procedure (Amplitude comparison)	41
Figure 4.7 :	A Pre-Breakdown-Region signature using the power spectrum analysis technique	42

Figure 4.8 :	A Pre-Breakdown-Region signature using the Correlation procedure method with 99 data points	43
Figure 4.9 :	A Pre-Breakdown-Region signature using the Correlation procedure method with 99 data points	44
Figure 4.10 :	Pre-Breakdown-Region signature comparison of Figures 4.8 and 4.9	45
Figure 4.11 :	A Pre-Breakdown-Region signature using the Correlation procedure method with 29 data points	46
Figure 4.12 :	A Pre-Breakdown-Region signature using the Correlation procedure method with 29 data points	47
Figure 4.13 :	Spatial dark conduction current before hydrogen ion implantaion	49
Figure 4.14 :	Spatial conduction current before hydrogen ion implantation, using a tungsten light source	50
Figure 4.15 :	Spatial conduction current before hydrogen ion implantation, using a tungsten light source with a red filter	51
Figure 4.16 :	Spatial conduction current before hydrogen ion implantation, using a tungsten light source with a green filter	52
Figure 4.17 :	Spatial conduction current before hydrogen ion implantation, using a tungsten	53

	light source with a blue filter	
Figure 4.18 :	Spatial dark conduction current after hydrogen ion implantation	54
Figure 4.19 :	Spatial conduction current after hydrogen ion implantation, using a tungsten light source	55
Figure 4.20 :	Spatial conduction current after hydrogen ion implantation, using a tungsten light source with a red filter	56
Figure 4.21 :	Spatial conduction current after hydrogen ion implantation, using a tungsten light source with a green filter	57
Figure 4.22 :	Spatial conduction current after hydrogen ion implantation, using a tungsten light source with a blue filter	58
Figure 4.23 :	Weight of four points on contact for all the data points taken	59
Figure 4.24 :	Scanning electron micrograph of a 0.3 μm thick silver layer formed on silicon wafer	62
Figure 4.25 :	X-ray spectra from the PIXE analysis at 40 MeV incident proton energy: (a) K x-rays from a Ag-Au alloy and (b) K x-rays	63

	from the silicon/silver target of the present study. The channel numbers and counts are proportional to the energies and the number of x-rays detected respectively	
Figure 4.26 :	XPS spectra of TiC(PS) coating subjected to $\approx$ 1500 plasma discharges inside the Tokamak fusion reactor. Intensity (CPS) vs. Kinetic Energy (ev).	64
Figure 4.27 :	XPS spectra of TiC(PS) coating subjected to $\approx$ 1500 plasma discharges inside the Tokamak fusion reactor. Intensity (CPS) vs. Kinetic Energy (ev).	65
Figure 4.28 :	Raman spectrum of the 60 KeV H_2^+ bombarded surface of TiC. Laser power 500 mW. Entrance slit-80 μ. Total data acquisition time - 6 hours. (multiple scans with 2 s/step)	67
Figure 4.29 :	Raman spectra of the TiC(PS) coating surface subjected to $\approx$ 1500 plasma discharges inside the Tokamak fusion reactor. Raman shift (cm^{-1}) vs. Intensity (CPS).	68
Figure 5.1 :	Scanning Electron Micrograph (100 x) shows total damage to the film after 100 keV hydrogen ion implantation. Bright spots are	76

from the substrate

ABSTRACT

Four ion implantation experiments undertaken at the University of Manitoba Accelerator Centre are discussed in detail. In the first experiment, three extreme conditions of aging effects for dielectric ISP under a high power environment have been isolated and simulated in laboratory. The three extreme conditions include : 1. H_2^+ ion bombardment, 2. electron irradiation of dielectric surfaces, and 3. localised heating. An ion accelerator, a spherical and a Gaussian electron discharge system, and thermal treatments are used for these simulations. Contributions to aging and their consequent effects on the dielectric have been monitored using a specially designed Four-Point Probe system and surface Raman scattering. The observations indicate that the H^+:H_2^+ ion bombardment causes a reduction of surface beakdown strength (to less than 1 % of its original value) and a reduction in surface resistance (by more than eight orders of magnitude) attributable to the fragmentation of long chain molecules on the surface and possible H related molecular formation on the surface as characterised by the Raman analysis of the surface. Results also show that post H^+:H_2^+ ion implantation annealing at T= 120^0C can not reverse the H^+:H_2^+ ion induced damage to the dielectric surfaces. On the other hand, H^+:H_2^+ ion bombardment does not affect the dielectric property of the bulk. Low energy electron (720 eV) irradiation also has no effect on the surface and bulk dielectric properties. The investigation of thermal aging effects from thermal breakdown experiments result in the discovery of a characteristic electical activity occurring prior to bulk dielectric thermal breakdown. The characteristic behaviour has been recognised using data processing techniques and a VAX/750 computer. The ability to

recognise this specular behavior is proved to be crucial to the prevention of thermal breakdown in the laboratory simulations. In the second experiment, a-Si:H thin films have been implanted with H^+:H_2^+ ions. Spatial conductivity measurements using a specially designed four point probe reveal a dramatic increase in photoconduction. This increase has been interpreted as due to the re-introduction of hydrogen into the low density interstitial region of the columnar microstructures of the films. The re-introduced hydrogen might have passivated some of the dangling bonds and damaged Si-O bonds. In the third experiment, a controlled and directed process for the deposition of silver film on semiconductor surfaces using the merit of energetic H^+:H_2^+ implantation is developed. The developed new technique eliminated any waste of the precious metal. Silver film deposited on the semiconductor surface is characterised with scanning electron microscopy and the presence of silver in the bulk of the semiconductor material below the surface is detected by the proton-induced X-ray emission (PIXE) technique. In the fourth experiment, TiC wafers of high purity, and TiC coatings deposited by a plasma spraying process were used to investigate the possibility of the formation of carbon-hydrogen and titanium-hydrogen complexes on the surface.

ACKNOWLEDGEMENTS

The author would like to thank his advisors Dr. J.S.C. McKee and Dr. M.S. Mathur for guidance and assistance in completing this work. He is also grateful to Manitoba Hydro for financial support throughout the period of his studies, and for the corporation's interest in the topics concerned.

Chapter 1 : INTRODUCTION

1.1 : H^+:H_2^+ Implantation Study of Dielectrics

Solid and fluid dielectrics are frequently used in high voltage systems. The effects of aging and environmental exposure on the dielectric properties of such materials is of major concern to power corporations. Since the environmental exposure causes surface effects, the study of the dielectric surface is important. The single most important effect of aging is directly related to the high voltage environment. It is well known that localised heating and therefore in some cases localised melting occurs for solid dielectrics under an intense electromagnetic force field because solid dielectrics are generally poor heat conductors (1-4). This study is undertaken to investigate dielectrics which are subjected to extreme aspects of a high power environment. The extreme conditions are isolated and simulated in the laboratory. The dielectrics used for the study are members of the urethane plastic family called ISP by its manufacturer and from now on will be referred to as dielectric ISP. The ISP is manufactured by DEXMAR and is a Toluene di Isocyanate resin. The ISP is provided by Manitoba Hydro.

To understand the reason for dielectric breakdown, three extreme conditions of the high power environment have been isolated and used to test on the dielectric ISP. The laboratory simulations of the actual conditions include:

i. H_2^+ ion bombardment of dielectric ISP surfaces. This experiment is performed under the assumption that, in a high power environment, hydrogen ions are generated as a result of lightning, flashovers, electrical discharges

and thunderstorms. The hydrogen ions thus generated impinge on the dielectric surfaces. To simulate the above situations, H_2^+ of up to 120 KeV are generated in the laboratory using the Narodny Ion Accelerator at the Accelerator Centre of the University of Manitoba (see Chapter 2 for details). 50:50 % of H^+:H_2^+ of desired fluences are allowed to bombard the dielectric ISP surfaces inside a high vacuum chamber.

ii. The irradiation of dielectric ISP surfaces with electrons emitted under an intense electromagnetic force field. For this, a spherical and a Gaussian discharge system have been built inside a less than one atmosphere environment. Electrons of up to 720 eV have been allowed to bombard the surface of dielectric ISP samples for periods up to 24 hours maximum.

On completion of the above two experiments, surface resistances are measured and the surfaces characterised using the technique of surface Raman light scattering. This technique establishes the formation of molecules and molecular complexes on surfaces. The data for H^+:H_2^+ implanted and electron irradiated surfaces are then compared with the data obtained for the surface of an unimplanted sample.

iii. The effect of changing temperature on bulk thermal conductivity of the dielectric ISP. Experiments such as this have a two-fold objective.

    a. It is well known that solid dielectrics under intense electromagnetic force fields are subject to localised heating inside the dielectrics, due to their poor heat conductivity. The first objective is to determine the bulk thermal conductivity and other thermal properties of the

dielectric ISP.

b. The second objective is to determine the effect of ion-implantation and electron irradiation on the bulk properties of the dielectric ISP. It was speculated that the injection of carriers during the irradiation might help in dissipation of heat, reducing the possibility of localised heating, thereby improving the bulk thermal breakdown strength of the dielectric.

1.2 : H^+:H_2^+ Implantation Study of a-Si:H Thin Film

It is well known that removal of hydrogen from a-Si:H leaves behind a high density of defects (5-7,9,10). It is also well known that ion implantation breaks bonds, blisters and distorts a surface and also creates defects (8,11,12). Therefore hydrogen ion implantation is believed to do more harm than good to a-Si:H film. Columnar microstructures resulting in strong anisotropic density fluctuations have long been considered a major class of defects in thin film depositions by evaporation (13), plasma-polymerization (14,15), dc sputtering (18) and by a range of different techniques (19). In the case of plasma-deposited a-Si:H films, Knights et. al. (16) have shown that the primary type of defect is in correlation with the columnar morphology of the film which results in density fluctuation and imperfect coalescence. Such columnar morphology identify by using scanning electron microscopy is believed to have existed even in the highest quality films. The interstitial regions between columns form a possible network of electrical defect centers, which invite rapid oxygen difusion into, and hydrogen difusion out of the regions. Therefore,

rapid oxidation and electrical defect formation will occur. Such phenomena cause aging of devices and discourage the use of plasma-deposited a-Si:H films in photovoltaic cells and other solid state devices. The purposes of the present experiments are as follows:

I to investigate the possibility of using hydrogen ions to penetrate low density interstitial regions without too much damage to the films themselves;

II to passivate the possible concentration of electrical defects;

III to prevent rapid oxidation;

IV to re-introduce hydrogen which has diffused out of the films;

V to densify the films; and hopefully,

VI to replace existing Si-O bonds with Si-H bonds. (some of the aged devices using device-grade a-Si:H films might be rejuvenated through H^+:H_2^+ implantation and it also might be possible to reduce defects even in high quality plasma deposited a-Si:H films).

1.3 : A New Technique of Electrical Contact Fabrication

Electrical contacts on a semiconductor surface are established either by the vapour deposition of a layer of conductive material or by implanting conductive metal ions. The latter of the two techniques is superior to the former because the former suffers from the fact that the contact between the semiconductor and conductor surface may be beset with interfacial problems. Whereas the conductive metal ion implantation results in structural bonding between the semiconductor and the metal ions, these two conventional methods are somewhat wasteful because the conductive

metal vapour has first to be produced and then unavoidably deposited on chamber walls and other components. A new technique has been attempted which utilises the implantation process without wasting Ag vapour.

The new technique ultilises energetic H^+:H_2^+ ions. Energetic H^+:H_2^+ ions in their journey towards the semiconductor surface go through a mask and a very thin silver foil. These energetic H^+:H_2^+ during collisions with the Ag atoms of the foil, transfer some positive charge to the foil and dislodge some Ag atoms/ions. If the semiconductor surface is negatively biased, a strong field will be established between the foil and the semiconductor surface. This field will accelerate the H^+:H_2^+ ions towards the substrate surface, and the flux of these accelerating H^+:H_2^+ ions will direct the dislodged Ag atoms/ions to the semiconductor surface. The H^+:H_2^+ will diffuse through the surface causing localised heating, whereas the impinging Ag atoms/ions will establish themselves on and slightly below the semiconductor surface. In this way, a conductive material surface is produced that is suitable for effective electrical contact.

1.4 : Plasma Interaction and Ion Implantation of a Refractory Material

H-H nuclear fusion requires a compatible condition to that of the interior of the sun. Such seemingly formidable conditions can be greatly reduced in D-T fusion (for example, a D-T fusion plasma requires a temperature in the order of $(10-20)\times10^7$ K). The D-T plasma can be confined by torroidal and poloidal fields, and energy confinement time is in the order of 1 sec., which for such a high temperature is a long time. Since there is no such thing as perfect confinement, plasma particles

unavoidably diffuse out of the plasma and impinge on the container wall and other components. Therefore, in the design of fusion reactors, the choice of material for the first wall, limiters and other components is rather critical. Energetic plasma ions can interact with these materials forming complexes, which, as impurities, degrade the plasma and lower its temperature. The surface of the exposed components will, of course, be altered in the process. As a result, materials chosen for the fusion reactor containment vessels and components should have: 1. high melting point, 2. resistance to thermal fatigue; physical and chemical sputterings. These desired characteristic make a TiC coating desirable for first wall applications. The present study investigates molecular formations on pure TiC wafers (99.95 % purity) and TiC coatings (by plasma spraying (PS) procedure (20)). In this chapter we are interested in the formation and absorption of carbon hydrogen and titanium-hydrogen complexes formed during H ion bombardment of the TiC (wafer and PS). In a similar experiment involving D^+:D_2^+ implantation of C (graphite), Mathur et. al. were successful in observing the formation and absorption of various deuterated methanes on the surface (21). These observations involved the use of the unenhanced surface Raman facility at the University of Kentucky. Conventional techniques involving low energy electron beams (Auger, LEED etc.) cause desorption of these complexes and prove somewhat ineffective (the formed complexes are often lost before the measurements commence). Use of the TFMS (Time of Flight Mass Spectrometry) technique is currently under investigation.

Chapter 2 : THE NARODNY ION ACCELERATOR AND THE SURFACE RAMAN FACILITY

This chapter describes in detail the two major existing facilities employed in the present study : (i) the Narodny Ion Accelerator at the University of Manitoba Accelerator Centre, (ii) the Inelastic Surface Raman Scattering facility at the University of Kentucky. Other experimental set-ups and systems built to carry on the study are described later.

2.1 : The Narodny Ion Accelerator

Shown in Figure 2.1 are portions of the linear accelerator used for the four surface implantation studies mentioned earlier. The linear accelerator, called the Narodny Ion Accelerator after its designer, has a unique acceleration energy range of 20 to 120 keV, with a beam current of ≈ 1 mA for H^+:H_2^+ ions. The maximum available beam current has been improved by the author to a value of $\approx$ 6 mA. Some major components of the accelerator are :

I an ion source capable of producing all type of common and noble gas ions.

II an extractor for directing the ion from source into the magnetic lens.

III a magnetic lens below the extractor which focuses the extracted ion beam into the acceleration column.

IV a fully shielded acceleration column (where the ions are accelerated to a desired energy), with a low gradient tube which employs cylindrical focussing

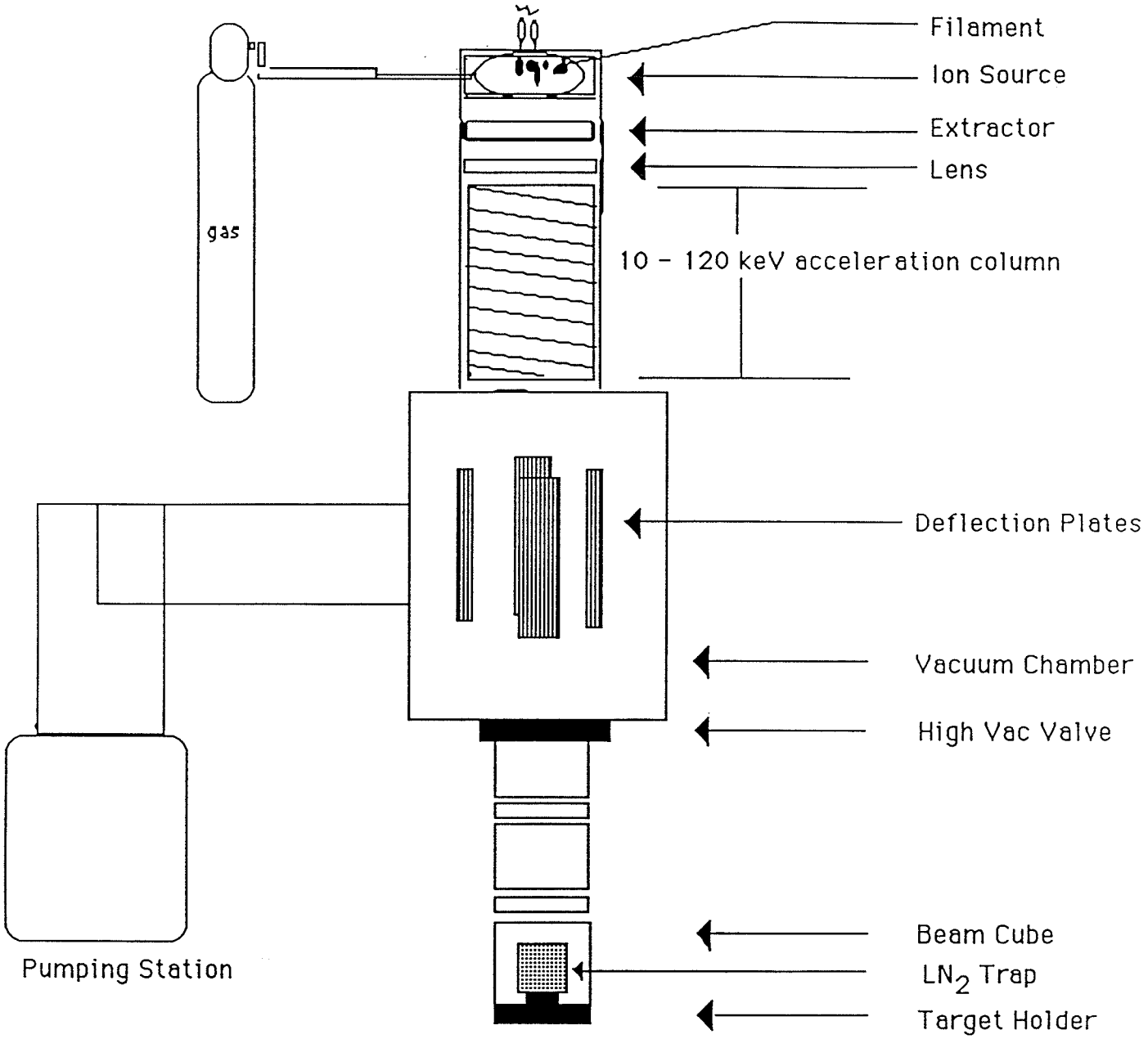

Figure 2.1 : Schmatic of the Narodny Ion Accelerator.

dynodes.

V a pumping station involving a 150 mm diffusion pump and a 1.6 m^3/min. roughing pump. A LN_2 cooled trap is installed around the target holder for most of the experiments to achieve a high vacuum in the order of 10^{-7} Torr and to keep the oil vapours away from the sample.

VI operation controls and main high voltage control system (not shown).

VII an IBM PC controlled ion beam scanning system with Metric threaded fasters for controlling the electrostatic deflection plates and changing the ion beam deflection in a pattern so as to achieve uniform implantation.

The desired fluence of implanted ions is derived from a knowledge of beam current, time of implantation and the area of the surface implanted.

2.2 : The Surface Raman Scattering Facility

Shown in Figure 2.2 is the schematic diagram of the surface Raman facility used for characterisation of implanted surfaces. The samples are mounted in a special chamber, where an Argon ion laser beam is incident on the sample at a very small angle. The light scattered from the surface and a few Å below the surface at 90^o to the incident light is analysed by a SPEX-1403, 0.85 m double monochromator and ECG and OMA data acquisition systems. New frequencies, generated by the interaction of vibrational frequencies of molecules and molecular complexes on the surface and the incident light, appear in observed spectra. The presence of these new frequencies establishes the formation or presence of molecules and molecular complexes on the surface.

SURFACE CHARACTERIZATION BY INELASTIC LIGHT SACATTERING

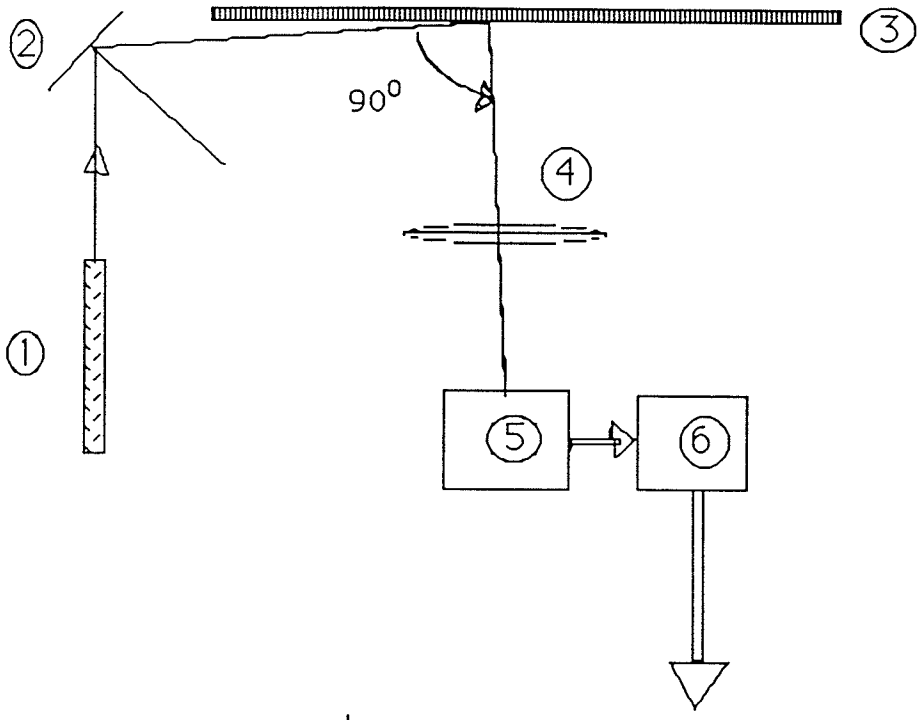

1 Ar^+ Laser 4885 Å

2 Front Surface Mirror

3 Sample Surface

4 Collection Optics

5 Double Monochromator

6 Data Acquistion System (S.P.C)

7 Surface Raman Spectrum

μ_o = Laser freq.

μ_s = Complex vib. freq.

Figure 2.2 : Surface Raman Light Scattering Facility.

Chapter 3 : EXPERIMENTAL DETAILS

3.1 : H^+:H_2^+ Implantation Study of Dielectrics

Both bulk and thin films of the dielectrics ISP have been exposed to an H^+:H_2^+ fluence ranging from 10^{16} to 10^{18} ions/cm^2. Three grades of the dielectric ISP have been obtained from chunks of the dielectric provided by Manitoba Hydro. Grade A is obtained from the outer region of the chunk, this is the best of all the grades obtained. Grade B is obtained from the central region and Grade C from the inner region, respectively. Small bubbles are observed in both Grade B and C with bubble diameters ranging from a few μm to 1.2 mm. The diameters of the bubbles increase from the outer region to the inner region progressively. The surface of Grade B was covered with 4 - 5 % and Grade C 13-15 % of the bubble voids. Dielectric ISP films of various thickness (40-260 μm) have been prepared following instruction from the Department of Geological Sciences. These thin films have been polished uniformly to a surface roughness of $\leq$ .3 μm (upper limit of surface microstructures). Each prepared film is then divided into three pieces. One for the unimplanted experiment and the other two for hydrogen ion implantation and electron irradiation respectively.

After hydrogen ion implantation and electron irradiation, surface conductivities are measured and compared with those of unimplanted samples. The experimental lay-outs for surface conductivity measurements are shown in Figure 3.1. Shown in Figure 3.1a is the specially designed 'Four-Point-Probe' (F.P.P.) system for spatial conductivity measurements and depicted in Figure 3.1b is the conven-

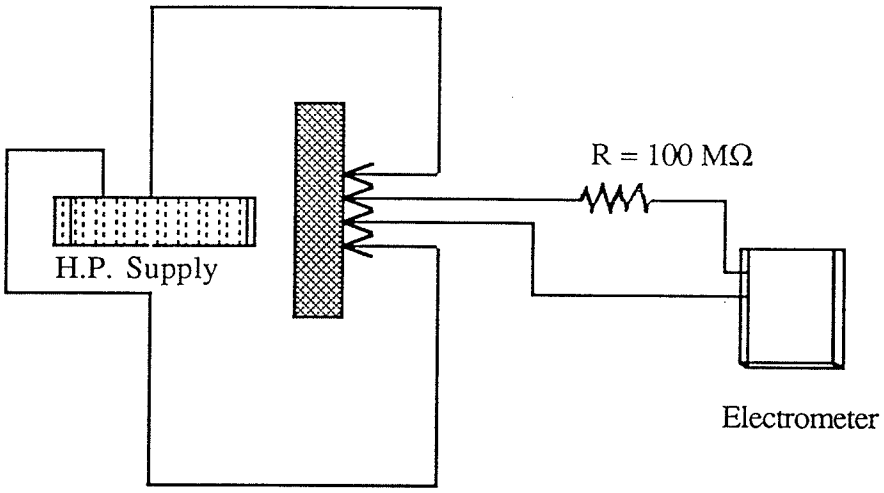

Figure 3.1a : Four-Point Probe System Set-up.

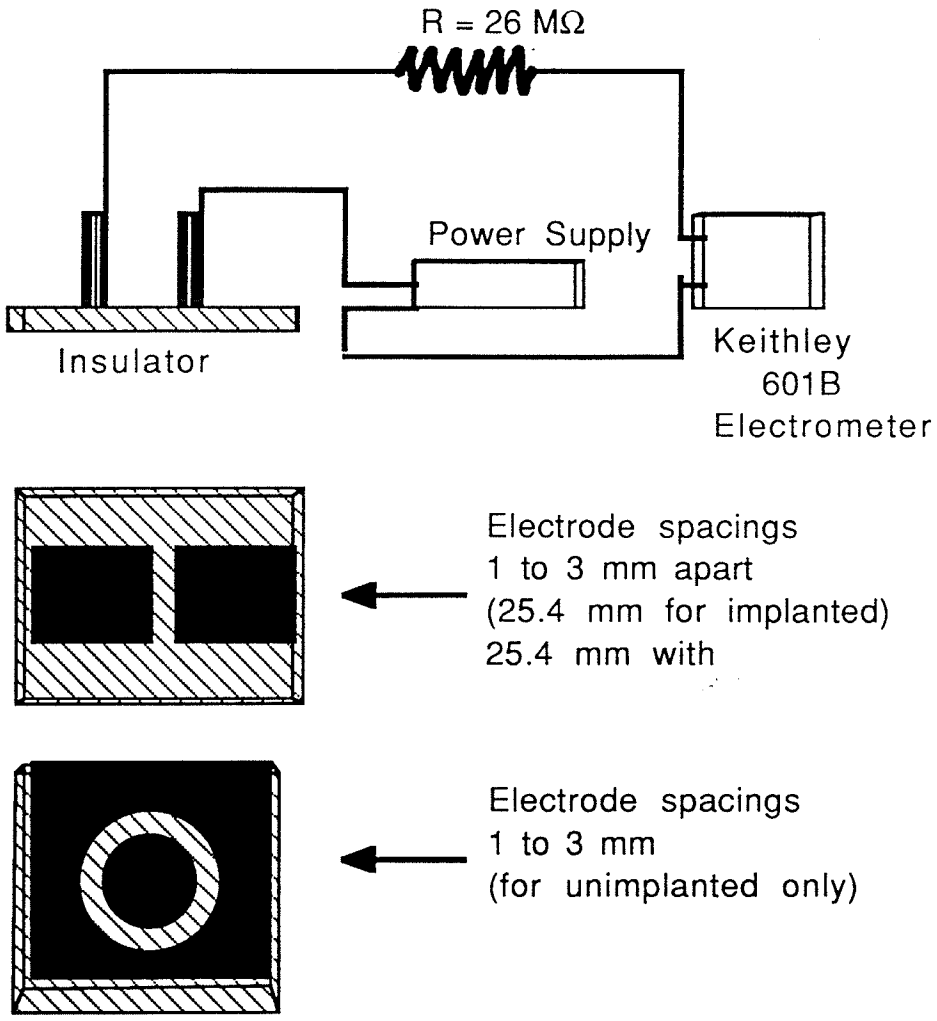

Figure 3.1b : Deposited-Electrodes Method.

tional 'Deposited Electrodes Method' (D.E.M.) which provides ohmic contact for the measurement. Both 'F.P.P.' and 'D.E.M.' measurements were undertaken to verify the validity of the results. The 'F.P.P.' is absolutely necessary because it is a non-destructive technique and some of the samples have to be preserved for the surface characterisations using the technique of inelastic Raman light scattering. The inelastic Raman light scattering is itself a non-destructive technique. As a result, bulk thermal breakdown experiments can be performed after surface characterisation. Therefore, surface breakdown experiments were performed only on the 'D.E.M.' samples. Another advantage of the 'F.P.P.' is the lack of noise generated by the fringing effects.

After the 'F.P.P.' measurements and surface characterisation, electrodes are deposited on these samples for bulk thermal breakdown experiments. For the 'D.E.M.', a simple but superior vacuum evaporated deposition system has been designed and built. Figure 3.2 shows the lay-out of this system where the vacuum chamber has been evacuated to less than 10^{-6} Torr using a 6 - inch diffusion pump and a LN_2 cold trap. Mathur et al have suggested a new technique of 'Ion-Assisted Deposition' (22) which will be discussed later. The surface characterisation of the unimplanted, H_2^+ implanted, and the electron irradiated dielectric ISP samples were undertaken employing the technique of inelastic Raman light scattering using the surface Raman facility at the University of Kentucky (described earlier). Inelastic Raman light scattering is a second order process (23) and the corresponding scattering cross-section is quite small ($\approx 10^{-34}$ m^2/molecules - steradian typically) and normally the counting rates for the adsorbed species are prohibitively small for routine

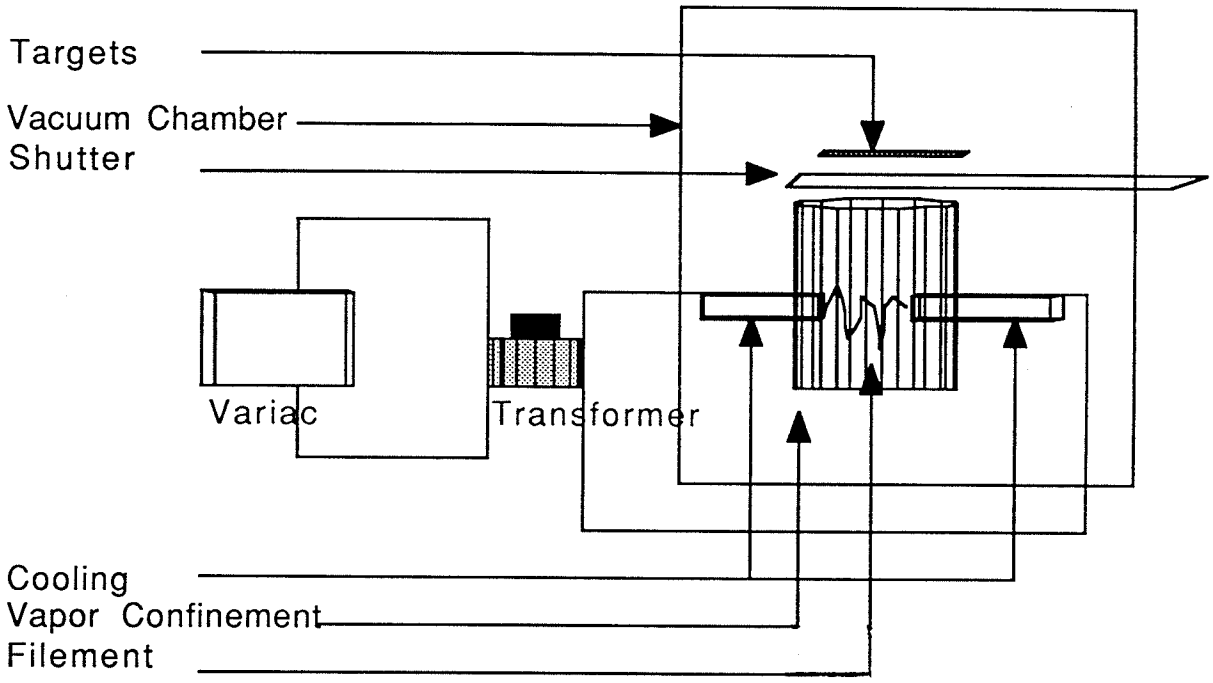

Figure 3.2 : High Vacuum Deposition System.

surface studies. However, with a system dedicated to study the Raman spectrum from low polarisability molecules adsorbed onto a poor Raman signal enhancer, characterisation of the surface adsorbed species has been successfully achieved (24). The detector system and data acquisition capability has been further improved for the present study.

The 500 mW output of the laser is further reduced at the sample because of the reflection and transmission losses in the laser beam transfer system and in the transmission filter used to remove the plasma lines thereby reducing the possibility of the desorption of the adsorbed molecules. Such lower laser power results in an extremely weak Raman scattered signal, and multiple scans over an extented period of time are needed for the present study.

Figure 3.3 shows a lay-our for the bulk thermal conductivity measurement. All of the unimplanted, implaned, and the electron irradiated dielectric ISP samples have been subjected to the thermal conductivity measurements.

3.2 : H^+:H_2^+ Implantation Study of a-Si:H Thin Film

a-Si:H films deposited on a quartz substrate by Electron Cyclotron Resonance (ECR) and plasma enchanced Chemical Vapour Deposition (CVD) were used for this experiment. An SEM micrograph example of columnar microstructure from one of the films is shown in Figure (3.4a). Figure (3.4b) gives a theoretical explanation for the formatin of the columnar microstructure. Fixed depositon conditions for the films are given in Table 1. Details of the ECR plasma enhanced CVD system are available in Ref. (17). The film thickness was measured with a Shoan Dektak me-

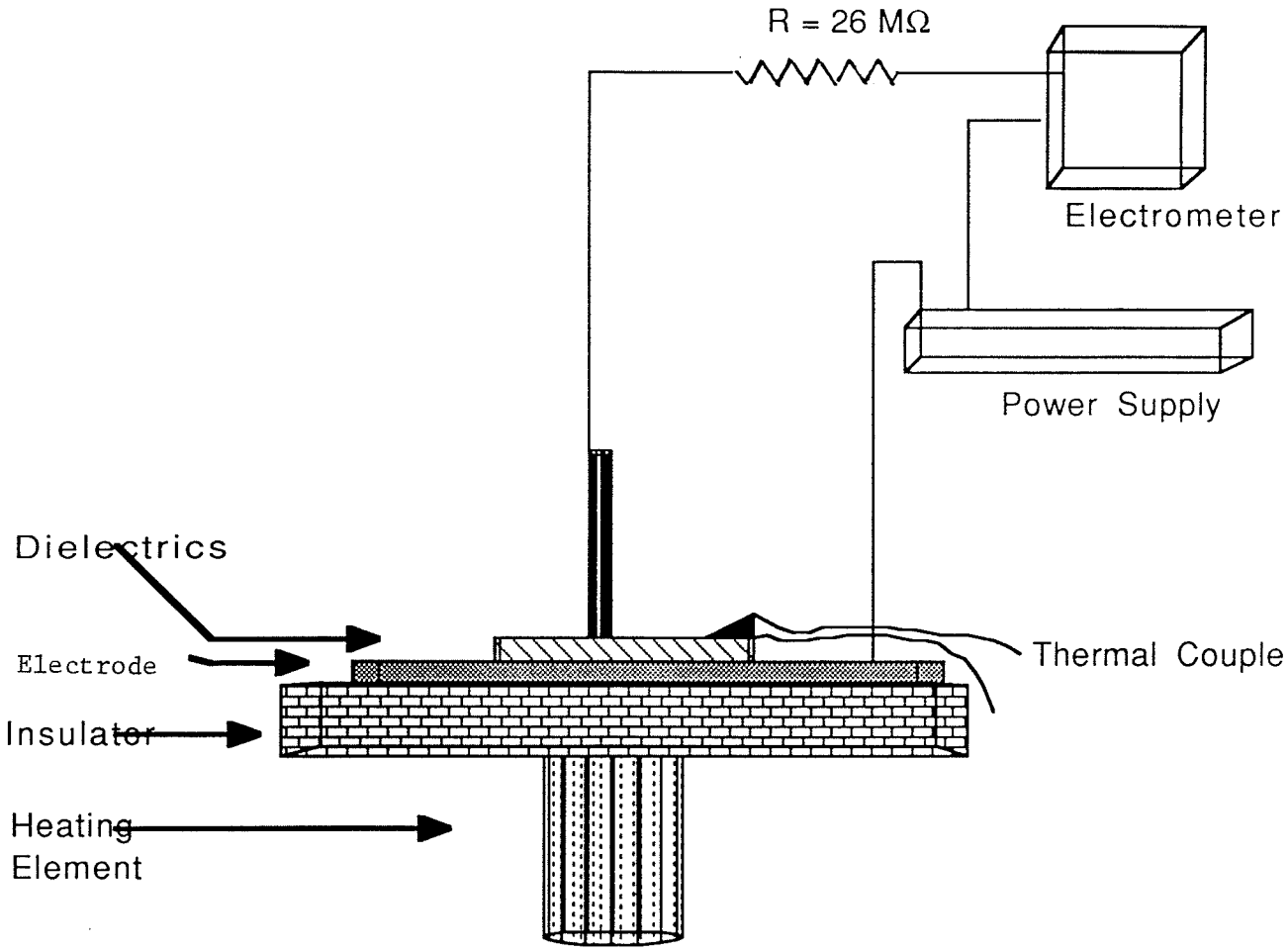

Figure 3.3 : Bulk Thermal Conductivity Measurement Lay-out.

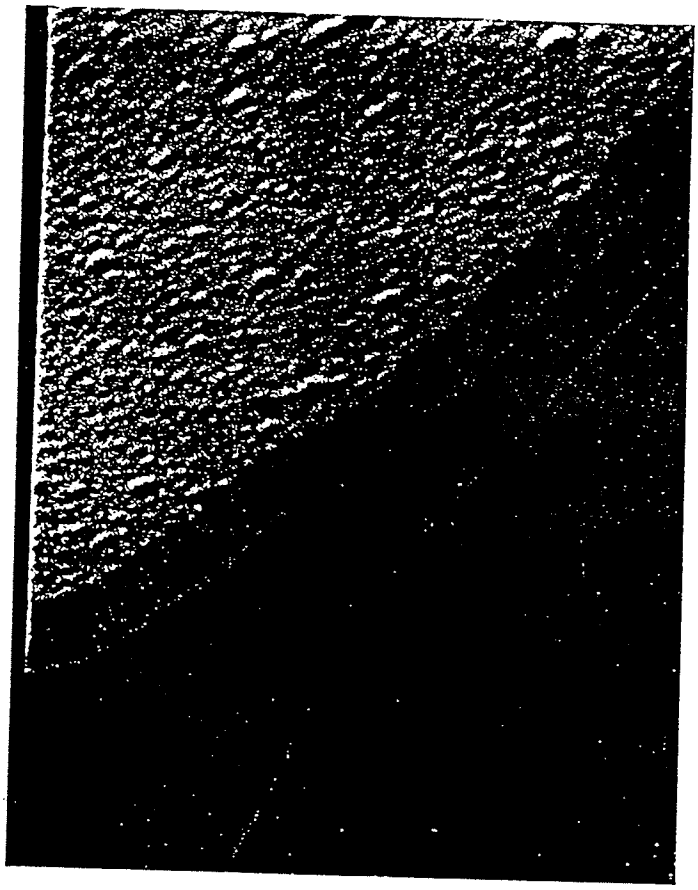

Figure 3.4a : Scanning Electron Micrograph of a-Si:H film 2000 x, shows an island-like features which extend all the way to the other side of the film, resulting in columnar morphology.

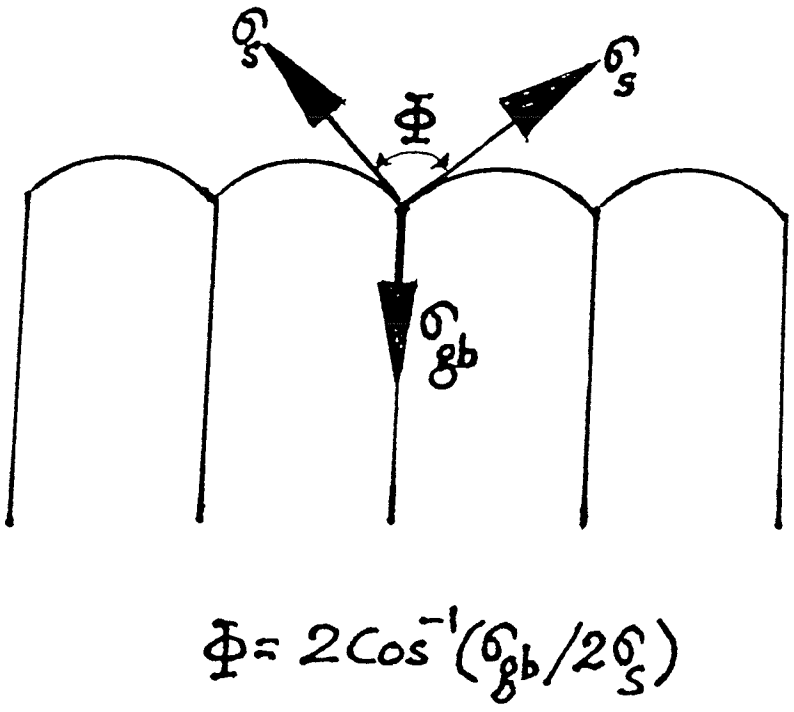

Figure 3.4b : Columnar profile of the a-Si:H film: Grain boundaries intersecting the growing surface modify the surface profile of the film. At the intersection of the grain boundary and surface, a grove with an opening angle Φ is formed where σ_{gb} and σ_s are the grain boundaries and the surface energy densities respectively.

chanical stylus instrument and was confirmed with ellipsometric and near infrared spectrophotometric measurements. Thickness of the a-Si:H films varied from 2.0 to 4.0 μm. Samples deposited were assessed to be amorphous by x-ray diffraction analysis both before and after H^+:H_2^+ implantation. Figure (3.5) shows a typical x-ray diffraction pattern.

TABLE 1

Deposition Parameters

Background pressure	10^{-6} Torr
Gas composition	10 % SiH_4, 90 % H_2
Gas total flow rate	22 sccm
Gas pressure	10–3 Torr
Microwave frequency	2.45 GHz
Microwave power absorbed	4 W
Magnetic field peak	$\approx$ 87.5 mT
Magnetic field strength	
at sample surface	$\approx$ 27.5 mT
Substrate bias	-300 V

A four point probe with inter-pole distance of 1 mm provided detailed spatial conductivity measurements before and after H^+:H_2^+ implantation over the desired experimental surface of the films. Reproducible conductivity measurements were made possible through a specially designed four point probe placed inside a high vacuum (HV) chamber, with spherical probe contacts of steel of known elastic constant to ensure the weight of contact. Other parameters, such

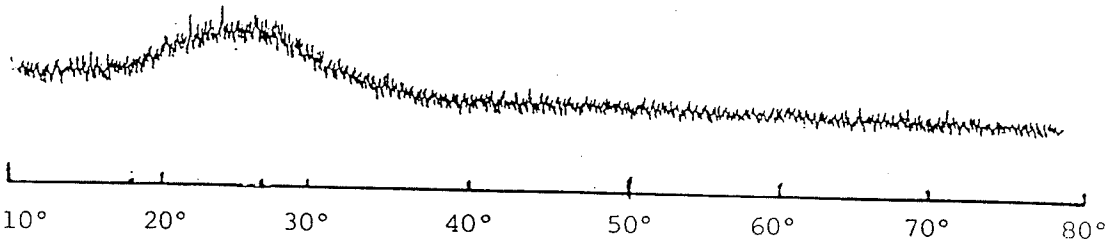

Fig. 2

Figure 3.5 : Typical X-ray diffraction pattern of an amorphous films employed in this study (Cu 40/20).

as chamber pressure, temperature, background conduction current and surface area on contact were held constant throughout the experiment. The whole set-up with its manual control was then placed in a bell-jar which was evacuated to a pressure of $\approx 10^{-6}$ Torr. Other constant parameters are given in Table 2. A dc voltage of 100 V was applied between the outer pair of probes and the inner pair was then connected to a Picoammeter for current measurement.

TABLE 2

Current Measurement Conditions

Chamber pressure	10^{-6} Torr
Temperature	25°C
Background current	1 – 2 pA
Apply dc voltage	100 V

The Narodny Ion Accelerator described earlier is used for hydrogen ion implantations of these films. A diffuse H^+:H_2^+ beam, with a LN_2 cool trap around the target area prevented overheating of the films and kept hydrocarbons away from the film surfaces. The number of H^+:H_2^+ ions implanted over a period of two hours was between 10^{16} to 10^{17} ions / cm^2. The implantation of H^+:H_2^+ ions of energy up to 30 KeV does not result in the crystallization, which is typical of X-ray diffraction. Table 3 lists the parameters of the accelerator in this implantation.

3.3 : A New Technique for Metal Contact Fibraction

The Narodny Ion Accelerator capable of producing gaseous ions of energies up to 120 keV is used to generate 80 - 100 keV H^+:H_2^+ ions for this experiment. The

sample mounting assembly is shown in Figure 3.6. The LN_2 cold trap around the sample holder keeps oil vapour away from the sample surface. The semiconductor

TABLE 3

Narodny Accelerator Irradiation Conditions

Acceleration energy	26.4 KeV
Duration	2 hrs
Pressure	1.2×10^{-5} Torr
Magnet Current	1 A
Lens Voltage	2 KV
Arc Current	0.6 A
Filament Current	30 A
Extractor Voltage	not working

(Si) wafer, silver foil and the mask combination is mounted in the sample holder as illustrated in Figure 3.6. The semiconductor is biased with - 90 to - 200 V. The energetic H^+:H_2^+ ions are allowed to impinge upon the combination of mask, silver foil and semiconductor wafer. The H^+:H_2^+ ions pass through the mask and foil, striking the semiconductor surface. Metal ions are dislodged and directed to the semiconductor surface where they establish a conductive region. Various combinations of H^+:H_2^+ energies and biasing voltages have been tried. After the implantation is complete, the samples are annealed and the surfaces are examined by a scanning electron microscope. The presence of Ag in the bulk of the semiconductor material is analysed by the proton induced X-ray emission (PIXE) technique at the Accelerator Centre. The working principle is the observation of the secondary X-rays

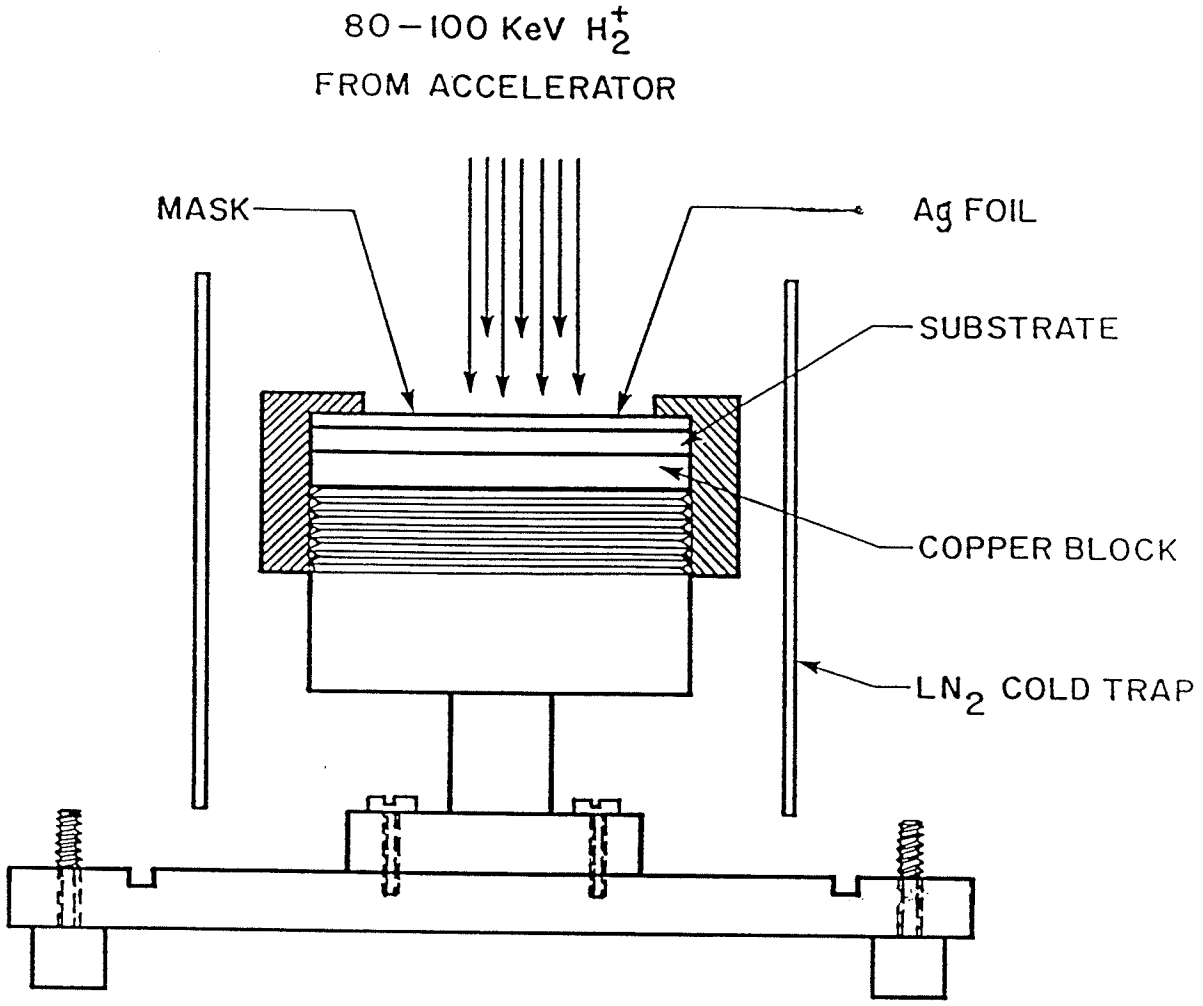

Figure 3.6 : Schematic representation of the target mounting assembly.

emitted when a proton beam (produced in the University of Manitoba cyclotron) passes through a thin target (24). In particular the incident beam energies are selected to produce maximum yields of K-shell X-rays for the element of interest (Ag here). As samples are being run, a computer gather data which are assembled into a spectrum with axes labelled 'counts' and 'channels'. These are respectively the number of X-rays detected at a particular energy and the X-ray energy itself is artificially divided into increments called channels. Each channel has an energy 'width' equal to full-scale energy divided by the number of channels, which in this experiment is about 20 eV. Based on a calibration standard, X-ray energies are derived from channel numbers corresponding to peak centres. Energies are compared with a chart of characteristic X-ray energies for various elements. The best fits are chosen and the elements identified. The intensity ratio between $K\beta$ and $K\alpha$ x-rays for a given element is also known and these values offer an additional means of confirming the presence of a particular elements. A typical experimental arrangement is given in Figure 3.7.

3.4 : Plasma Interaction and Ion Implantation of Refractory Materials

The TiC wafers of 0.0254 m diameter, and 0.003 m thickness are acquired from the Atomergic Chemical Corporation of New york. These wafers have 99.95% purity, and in order to avoid contamination the wafers are kept under vacuum until the time of experiment. The TiC coatings of 300 to 400 μm thickness were prepared at the Institute de Genie des Materiaux (Bou Cheville, Canada) by plasma spraying

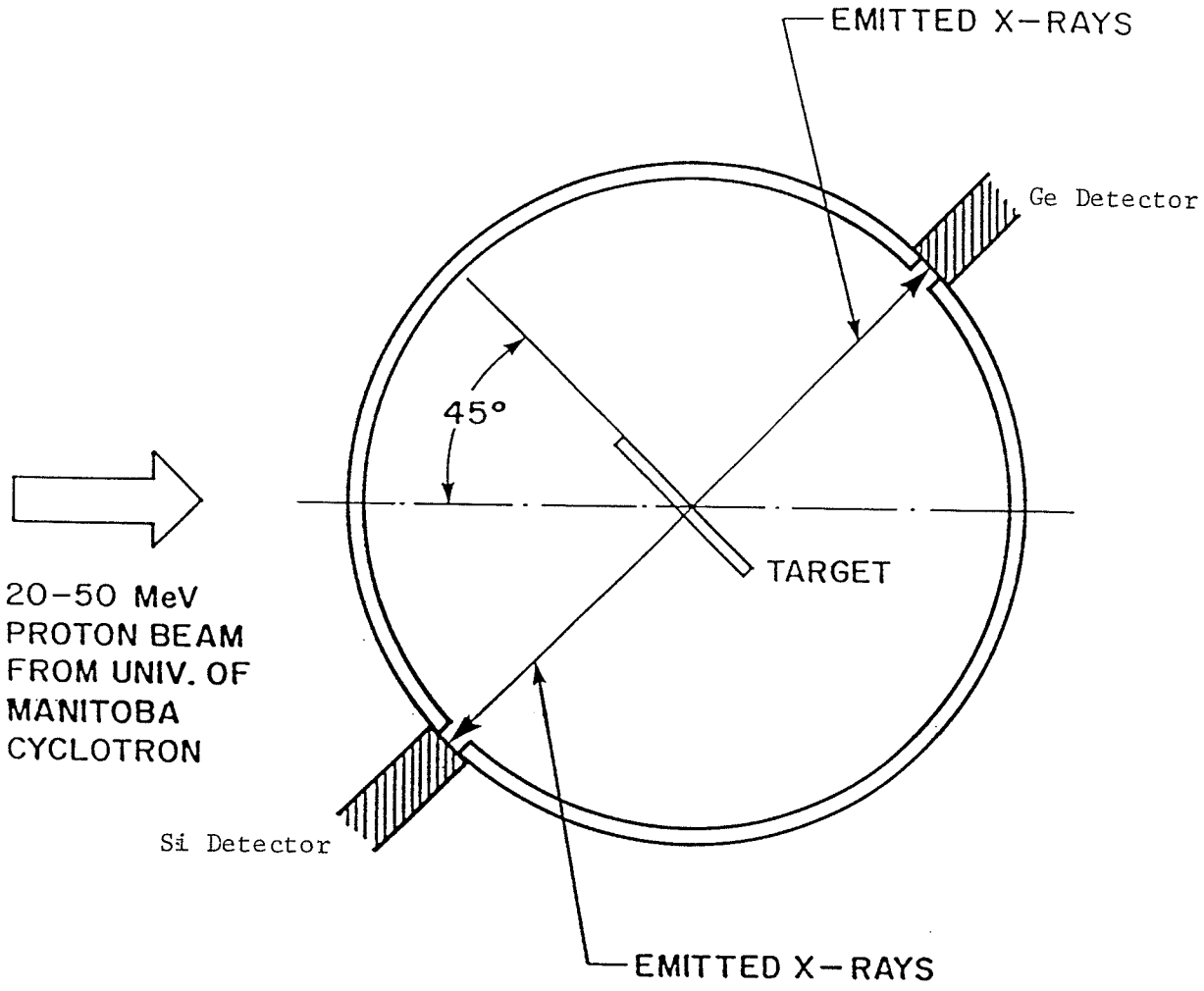

Figure 3.7 : Experimental arrangement for PIXE analysis.

onto Inconel 624 substrate (25). These coated samples were placed on the internal wall of the Tokamak fusion reactor and were subjected to repeated hydrogen plasma discharges. The samples were left inside the reactors for three months or $\approx$ 1500 discharges and were sealed in positive hydrogen pressure environment upon removal from the reactor. H^+:H_2^+ ions of 60 keV were generated using the Narodny Linear Accelerator and bombarded the surface of the TiC wafers. The wafers were mounted in a specially designed sample holder, and the sample was surrounded by the LN_2 cold trap to keep pump oil vapours away from the sample surface. A beam of energetic H^+:H_2^+ passed through a deflection plate assembly, whereby the beam was deflected across the surface of the target thus scanning the surface under computer control. Beam diameter and beam current were measured and the wafer were exposed to the beam for a known period of time to achieve uniform implantation. The desired fluence of particles was calculated using:

$$\text{number of ions/cm}^2 = 1.6 \times 10^{-19}\ (\text{I/A})\text{t}.$$

Where I was current in Ampere, A the implanted area in cm^2 and t the time in seconds. During the entire experiment, a vacuum of 10^{-7} Torr was maintained in the system. After implantation, the TiC wafer was transferred immediatelly to a holder where it was kept under positive H_2 pressure. The sample was removed from this hydrogen environment prior to surface analysis.

The Kratos surface analysis system at the University of Kentucky was used to perform XPS (X-ray photoelectron spectroscopy) and characterization of the surface of TiC (PS) and TiC wafers also employed the use of surface Raman facility.

Chapter 4 : OBSERVATIONS AND RESULTS

4.1 : H^+:H_2^+ Implantation Study of Dielectrics

The Raman spectrum of the unimplanted surface of the dielectric ISP is given in Figure 4.1a. Except for the small amount of fluorescence as is evident by the non-linearity in the background, no Raman activity is evident. The Raman spectrum of a dielectric ISP surface which has been bombarded with 30 KeV H^+:H_2^+ ions to a fluence of 10^{16} ions/cm^2 is shown in Figure 4.1b. Raman bands at 1040, 1276, 1316, 1620, 1738, 2876, 2938 and 3066 cm^{-1} indicate that the H^+:H_2^+ implanted surface is alive with a significant amount of molecular activity. Toluene di Isocyanate X-N=C=O, where X is methyl benzene (toluene) could have ortho, meta and para structures. Vibrational assignments in the Infrared (IR) and Raman spectra of isocyanic acid have been observed by Herzberg and Reid (26). The pseudo antisymmetric NCO stretch ν(sym) (N=C=O) occurs in the Raman spectrum of the liquid at 1318 cm^{-1}. Assignments of the fundamental modes of vibration of methyl isocyanate have been made by Hirschmann, Kriseley, and Fassel (27). The benzene ring stretching vibration occurs in the Raman spectrum at 1310 cm^{-1}. Hence the observed 1316 cm^{-1} Raman band could be a combination of N=C=O pseudo symmetric stretch and the benzene ring stretching vibration. The 1280 - 1240 cm^{-1} Raman band is normally attributable to the ring stretching vibrations and our 1270 cm^{-1} Raman band can thus be assigned to such a vibration.

The 2938 and 2876 cm^{-1} levels form a Fermi doublet through the interaction of the overtone of CH_3 asymmetric deformation mode at 1456 cm^{-1}. The CH_3

Figure 4.1a : Raman spectrum of H_2^+ unimplanted Dielectric 'ISP'.

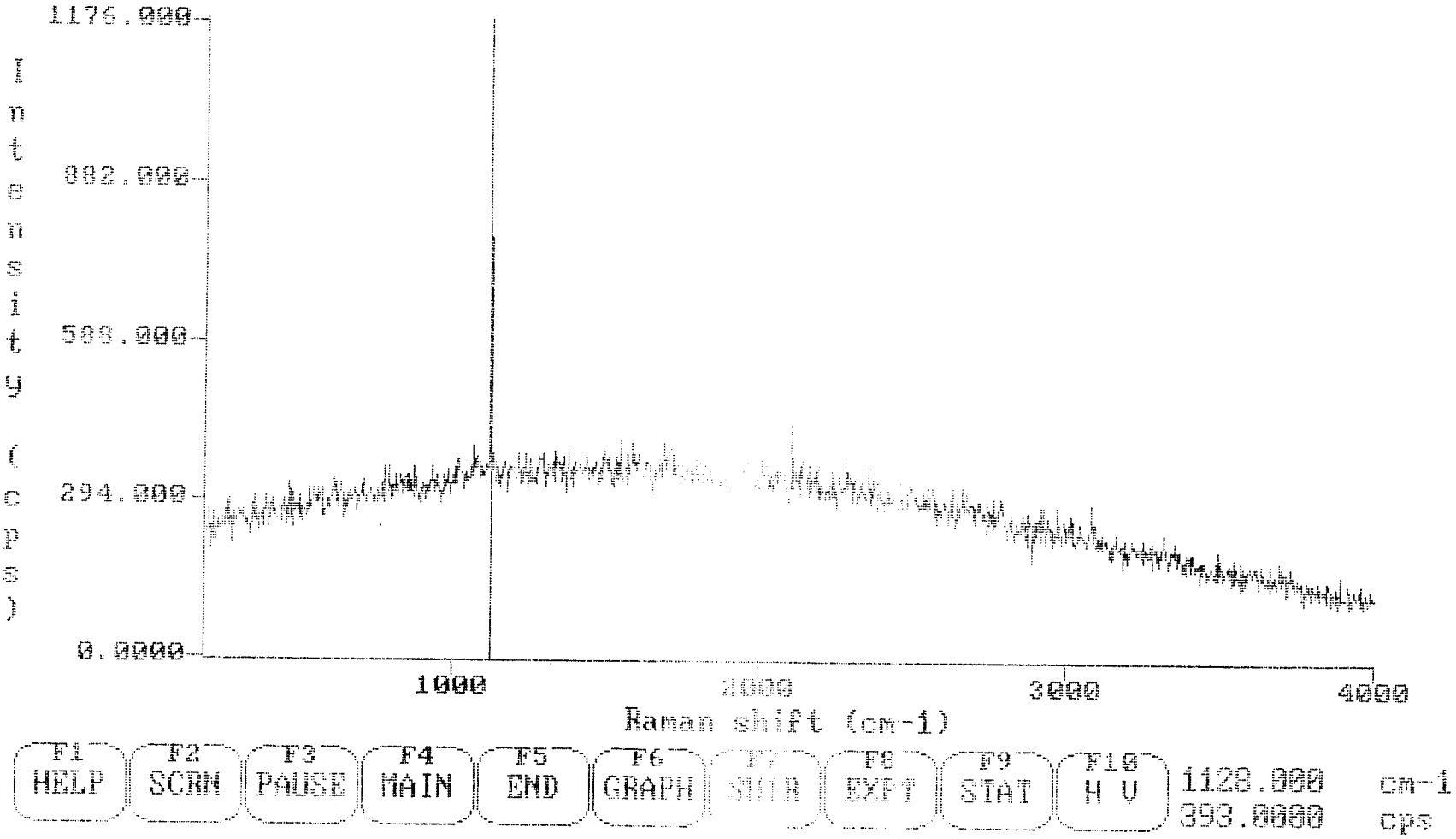

Figure 4.1b : Raman spectrum of H_2^+ implanted dielectric 'ISP', part I.

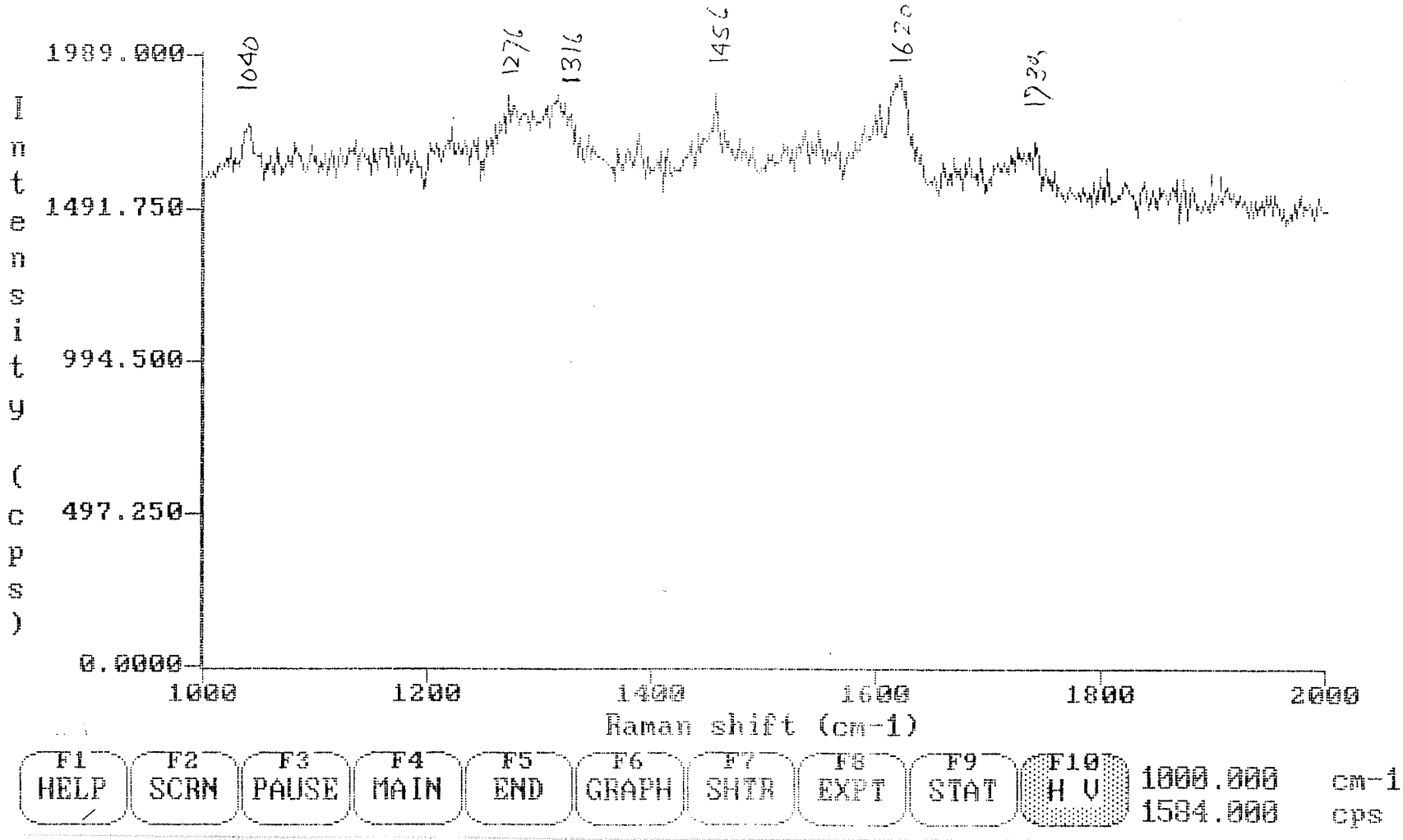

Figure 4.1b : Raman spectrum of H_2^+ implanted dielectric 'ISP', part II.

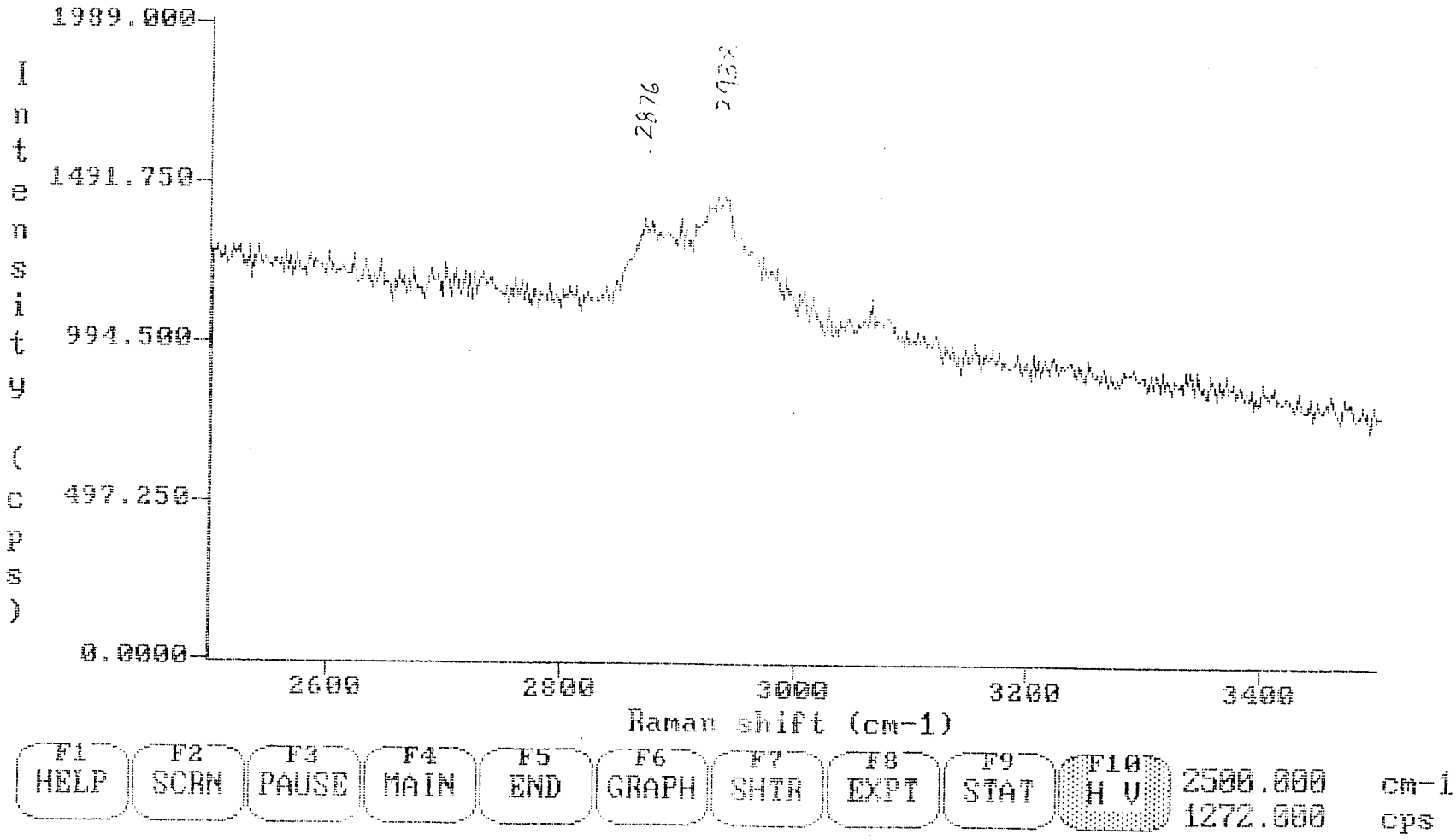

group has a normal frequency of about 1450 cm^{-1} and occurs in our study at 1456 cm^{-1}. The C-H doublet centered at 1600 cm^{-1} also occurs in the Raman spectra of these derivatives (28). In our study these frequencies occur at 3066 and 1620 cm^{-1} respectively. The 1738 cm^{-1} Raman band in our spectrum can be assigned to the C=O stretching and the CH bond bending vibration of CH_3 occurs at 1000 cm^{-1} (29). The 1040 cm^{-1} Raman band in our observations can be attributed to such a vibration.

The Raman spectrum of the H^+:H_2^+ implanted dielectric ISP resin surface indicates that a considerable amount of molecular activity is taking place on the surface. The characteristic vibrations of the CH_3 group, N=C=O group and the benzene ring have been identified. This suggests that the hydrogen ion bombardment is causing dissociation of the long molecular chains of the dielectric into smaller segments. Once these segments are free from the constrains of the long chain, their individual vibrational acitivity becomes prominent. This molecular activity results in the Raman spectrum. It is likely that the dissociation of the long chains into segments might also be responsible for the surface breakdown behaviour of the dielectric ISP as will be presented later. The individual segments or fragments have different dielectric properties to those of the long chain delectric ISP. Hence the observation of the Raman activity on the bombarded surface is an indication of the surface dielectric breakdown.

Figure 4.2 shows a characteristic voltage vs. surface current variation for the implanted dielectric ISP with H^+:H_2^+ ion fluences between 10^{16} to 10^{18} ions/cm^2. Dielectric ISP implanted with hydrogen ions within the above range of fluence

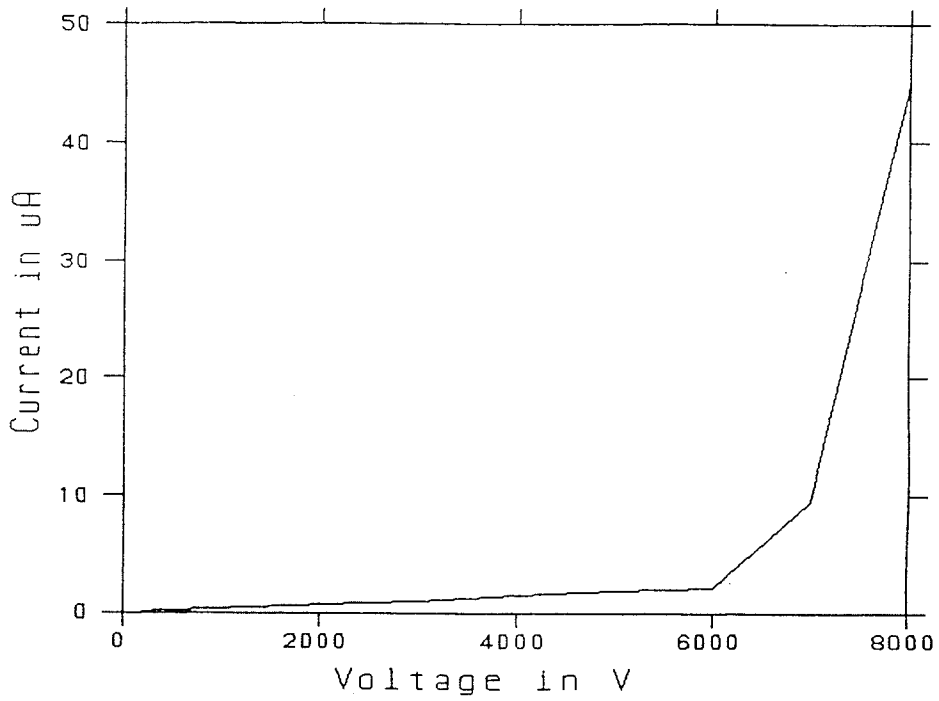

Figure 4.2 : Typical voltage vs. surface current plot for the H_2^+ implanted dielectric 'ISP'.

exhibits a detectable surface current for almost any applied voltage (in a sense the implantation turns dielectric ISP surfaces into conductor). Measurements such as this indicate that the introduction of hydrogen ions into dielectric ISP resulted in a reduction of surface resistance by more than eight orders of magnitude, in some cases, even more than eleven orders of magnitude are recorded. A reduction in surface breakdown strength to less than one percent of the original value is also observed. When the applied voltage reaches a value of 6,000 V, surface current begins to increase in an exponential fashion, indicating that breakdown will occur at this applied voltage if enough time is allowed. Post implantation annealing at various temperature of up to 120 ^{0}C under atmospheric pressure could not reverse any of the above effects. On the other hand in the case of unimplanted dielectric ISP surfaces and the electron irradiated surfaces, no detectable electrical activity is recorded for applied voltages of upto 10 kV Maximum (the upper limited of the high voltage supply used for the experiment). In spite of a visible change in the surface texture of the electron irradiated dielectric ISP, no modification in the surface conductivity and surface breakdown strengths is observed.

Figure 4.3 shows a typical bulk thermal conduction leading to break down when applied field is kept constant. Such behaviour is similar for all the unimplanted, implanted, and the electron irradiated samples of the dielectric ISP. Figure 4.4 shows the time rate of temperature change of the Figure 4.3 at a constant applied field of 2,500 V. Figure 4.2 can be divided into four regions:

a. The first region is designated as the 'Non-Active Region' (N.A.R.) where no detectable electrical activity was observed.

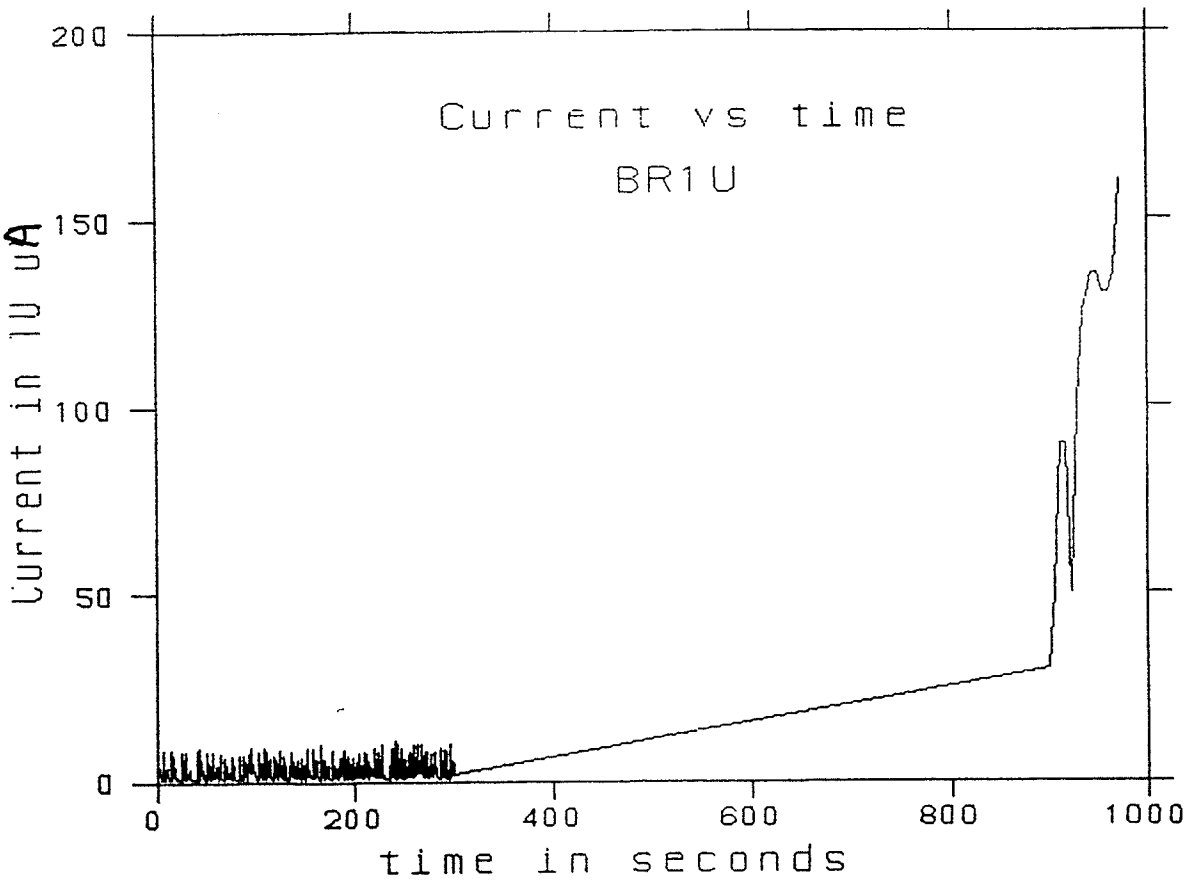

Figure 4.3 : Characteristic bulk thermal breakdown at constant applied field.

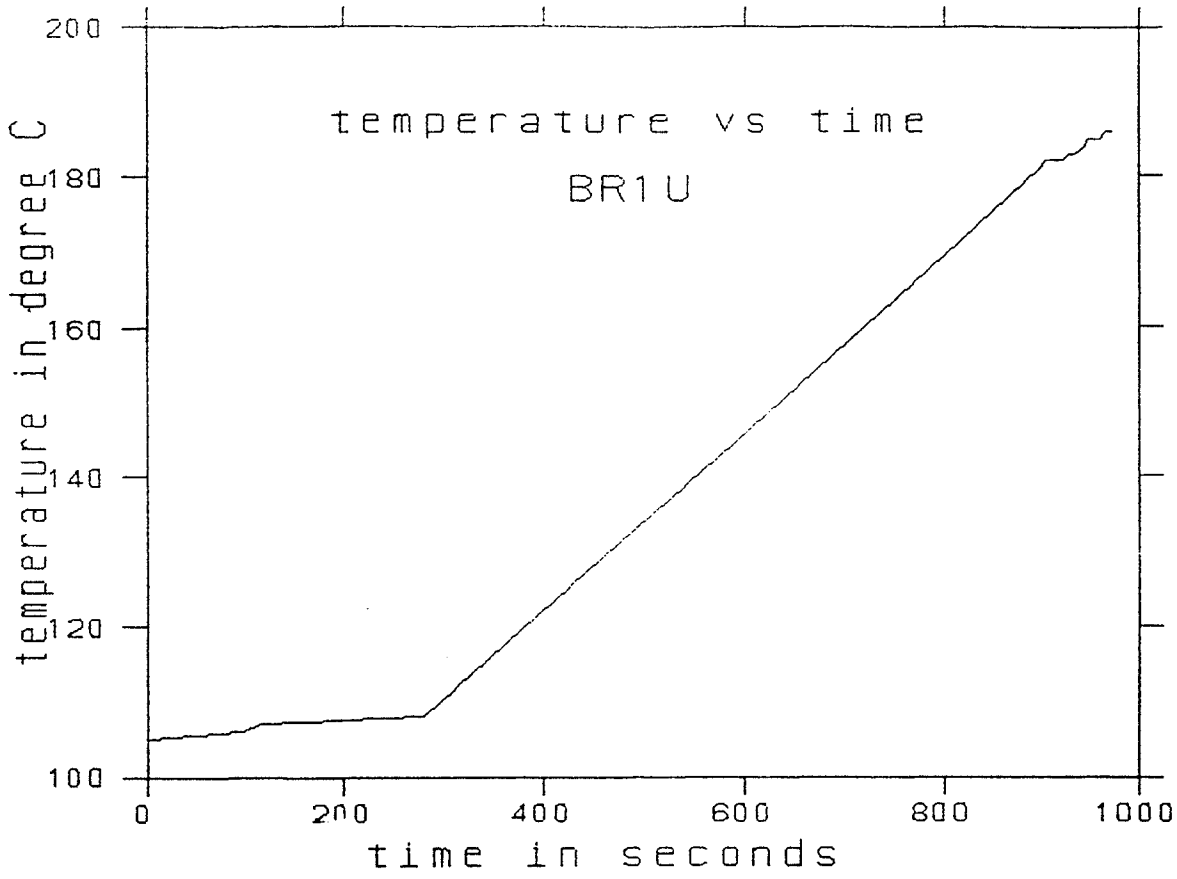

Figure 4.4 : Temperature vs. time variation of Figure 4.3.

b. The second region is designated as the 'Pre-Breakdown Region' (P.B.R.); in the 'P.B.R.', electrical, as well as thermal processes are reversible and no modification to the dielectic properties of the ISP takes place. Therefore, thermal breakdown can be prevented in this region by lowering the applied field, while keeping the temperature constant, or lowering the temperature and keeping the applied field constant, or lowering both the temperature and the applied voltage.

c. The third region is designated as the 'Transition Region' (T.R.). Detailed investigations are needed to understand the actual physical state of the dielectric ISP in this region. We hope to be able to continue this investigation using 'Power Spectrum Analysis' (P.S.A.), the 'Maximum Entropy Method' (M.E.M.) and the 'Maximum Likelihood Method' (M.L.M.) procedures to determine the actual electrical and thermal states of dielectric ISP in this region.

d. The fourth region is designated as the 'Breakdown Region' (B.R.), where permanent modifications to the electrical and physical properties of the dielectric ISP have occurred. As a result, breakdown can not be prevented in this region.

Figure 4.5 shows how breakdown can be prevented from the 'P.B.R.' by lowering the temperature at a constant applied voltage of 2,500 V. It is evident that the specular behaviour of the electrical activity of the dielectric ISP in this 'P.B.R.' is important for power system analysis. The ability to recognise dielectrics in this state is critical to prevent breakdown from materialising. Considering the

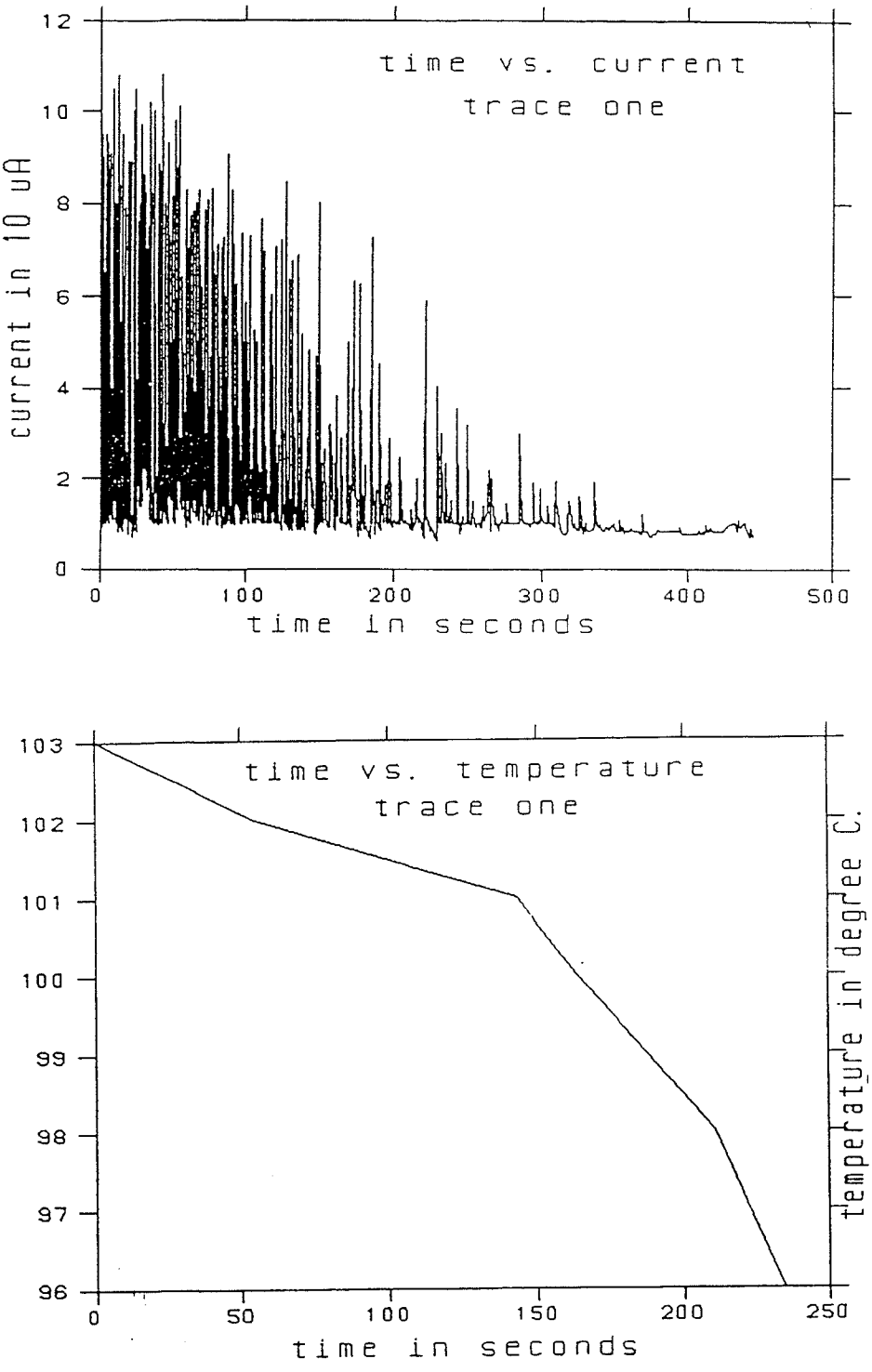

Figure 4.5 : Breakdown prevention from the Pre-Breakdown-Region at constant applied voltage.

importance of such specular behaviour in the 'P.B.R.', algorithms have been developed and translated into Fortran Procedures using the VAX/750 computer to automatically recognise the presence of the 'P.B.R.'. The preliminary results indicate that using a 'Fast Fourier Transform' (F.F.T.) procedure, the VAX/750 is capable of recognising the 'P.B.R.' as shown in Figure 4.6. On the other hand, using the 'P.S.A.', a more indicative signature is obtained from the computer, as shown in Figure 4.7. The most promising algorithm is the use of what we refer to as 'Correlation Procedures' (C.P.) using 'Convolution at Norm', 'Convolution at F.F.T.'. and 'Convolution at IFFT (Inverse F.F.T.)'. Figure 4.8 shows how the 'P.B.R.' is recognised with only 99 data points sampled from a thermal breakdown experiment in the 'P.B.R.'. This signature is verified with same amount of data points sampled from another experiment performed under similar conditions. Shown in Figure 4.9 is the signature for this experiment and Figure 4.10 shows the Figures 4.8 and 4.9 together for comparison. Similar correlation was obtained with a minimum of 29 data points sampled from two other experiments (Figures 4.11-4.12); as expected, the results are identical to that of Figure 4.10, indicating the superiority of the 'C.P.' for recognising the deterministic 'P.B.R.'. A continuation of this investigation is proposed to monitor electrical and thermal state *in situ* in real time analysis using only a micro-computer system. Such prototype micro-computer monitorring system shall be capable of multi channel, multi-device and multi-situation simultaneous analysis.

4.2 : H^+:H_2^+ Implantation Study of a-Si:H Thin Film

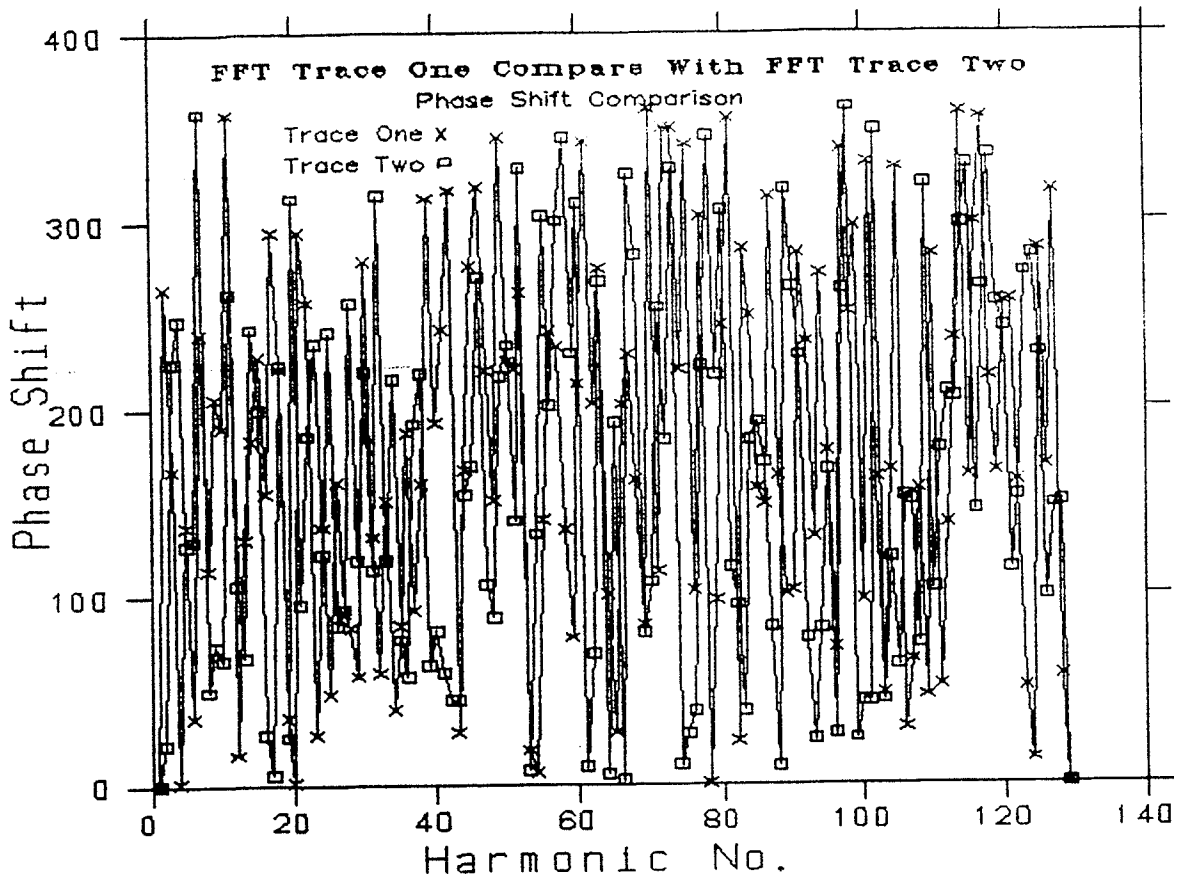

Figure 4.6a : Pre-Breakdown Region signature comparison using FFT procedure (Phase Shift comparison).

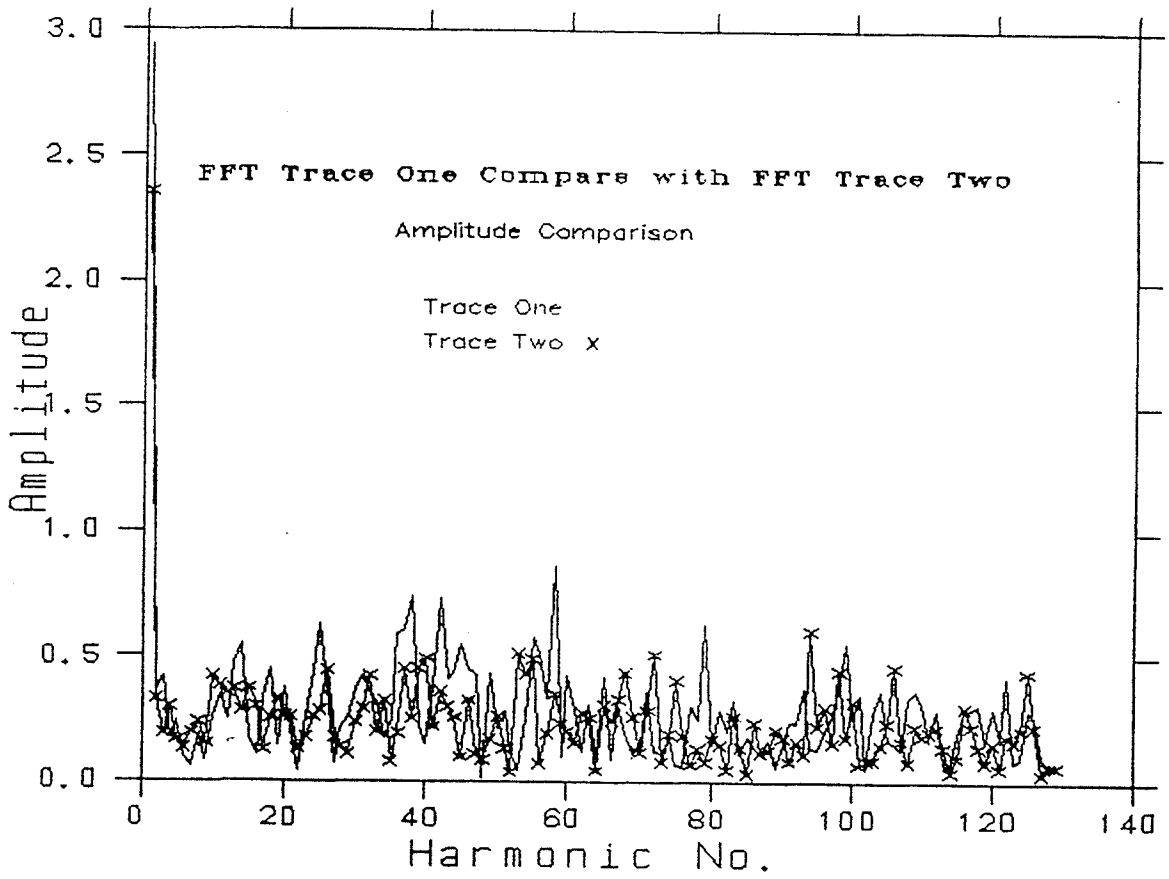

Figure 4.6b : Pre-Breakdown Region signature comparison using the FFT procedure (Amplitude Comparison).

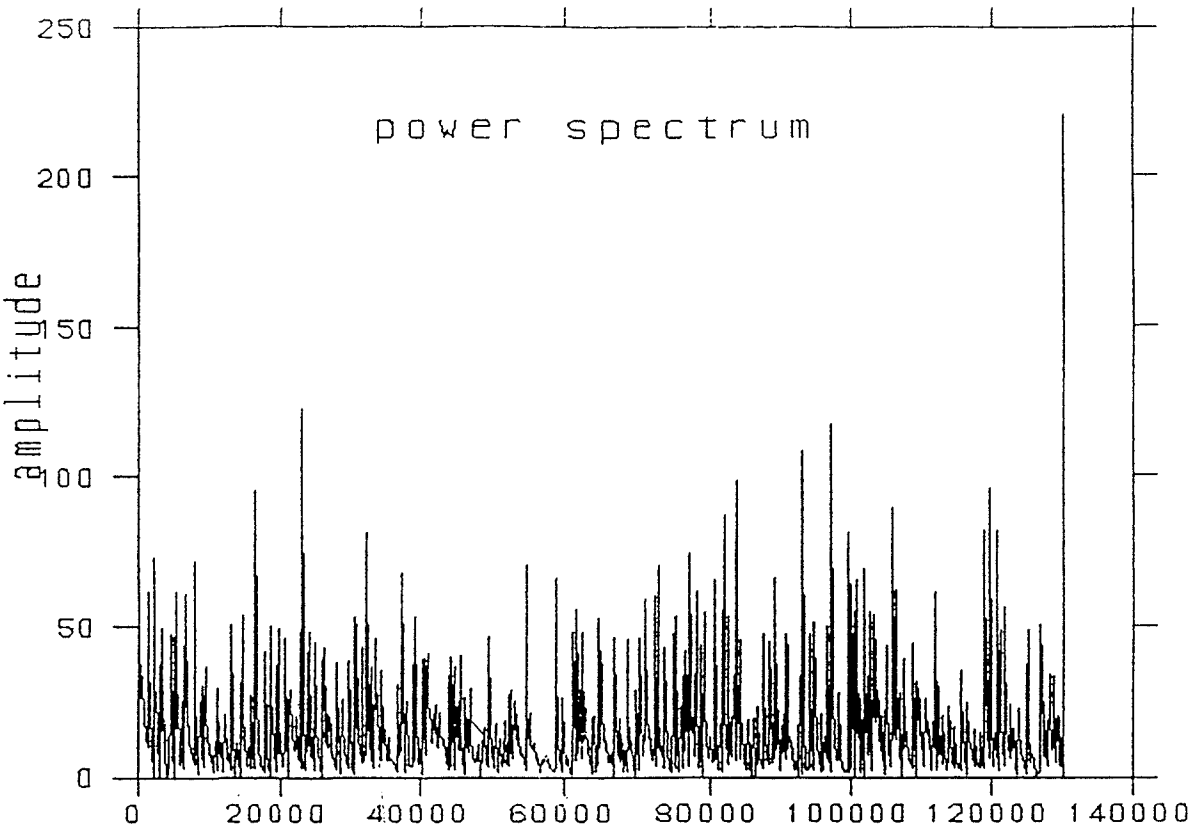

Fgiure 4.7 : A Pre-Breakdown Region signature using the power spectrum analysis technique.

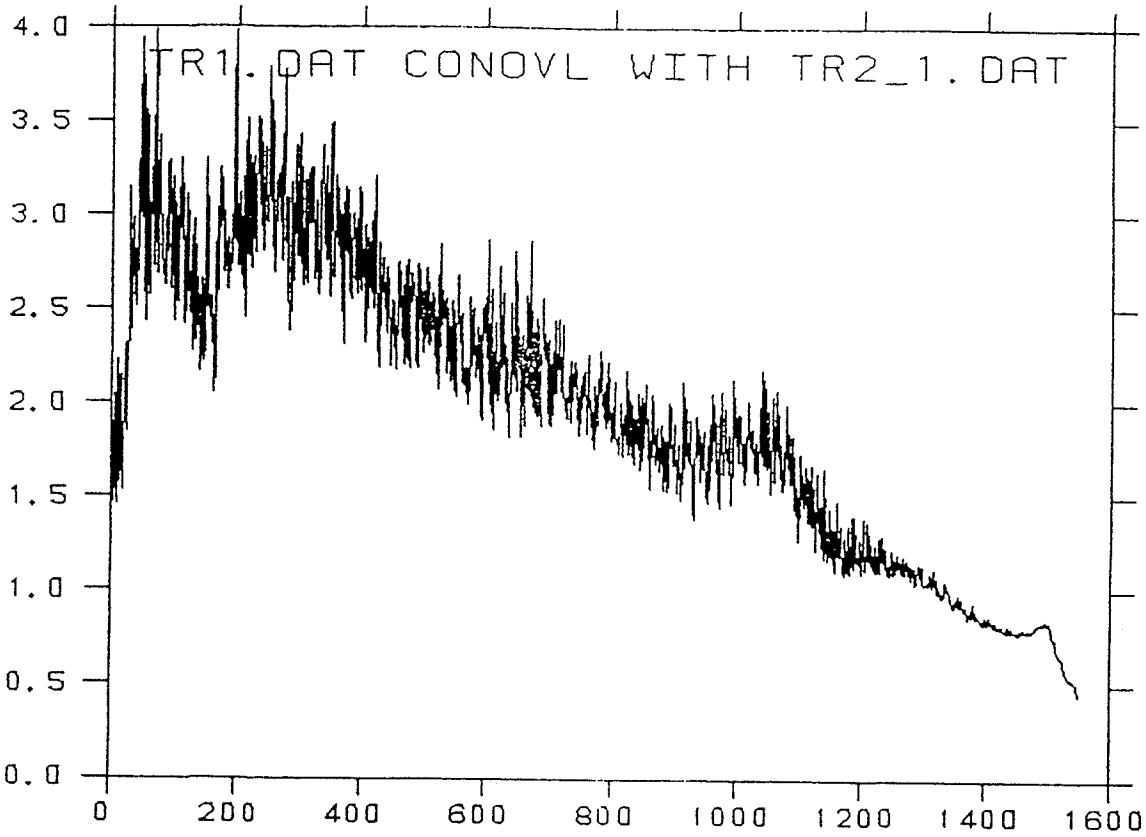

Figure 4.8 : A Pre-Breakdown Region signature using the Correlation Procedure Method with 99 data points.

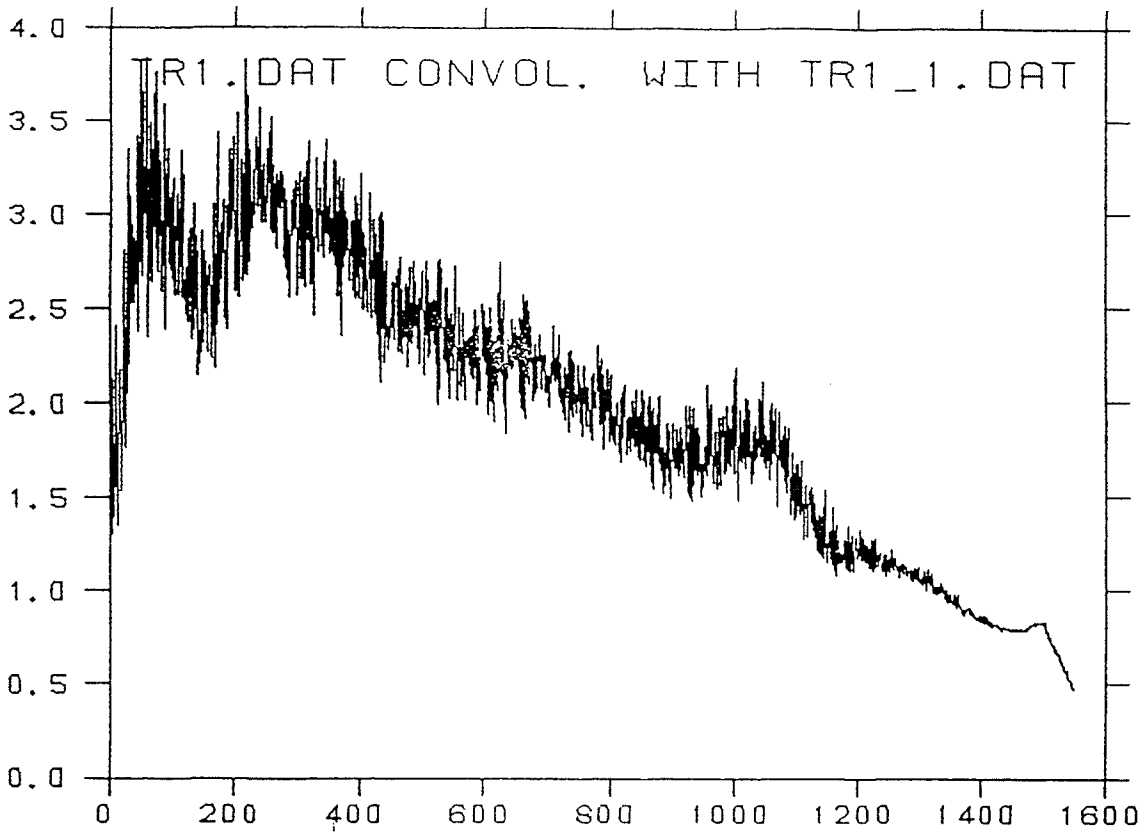

Figure 4.9 : A Pre-Breakdown Region signature using the Correlation Procedure Method with 99 data points.

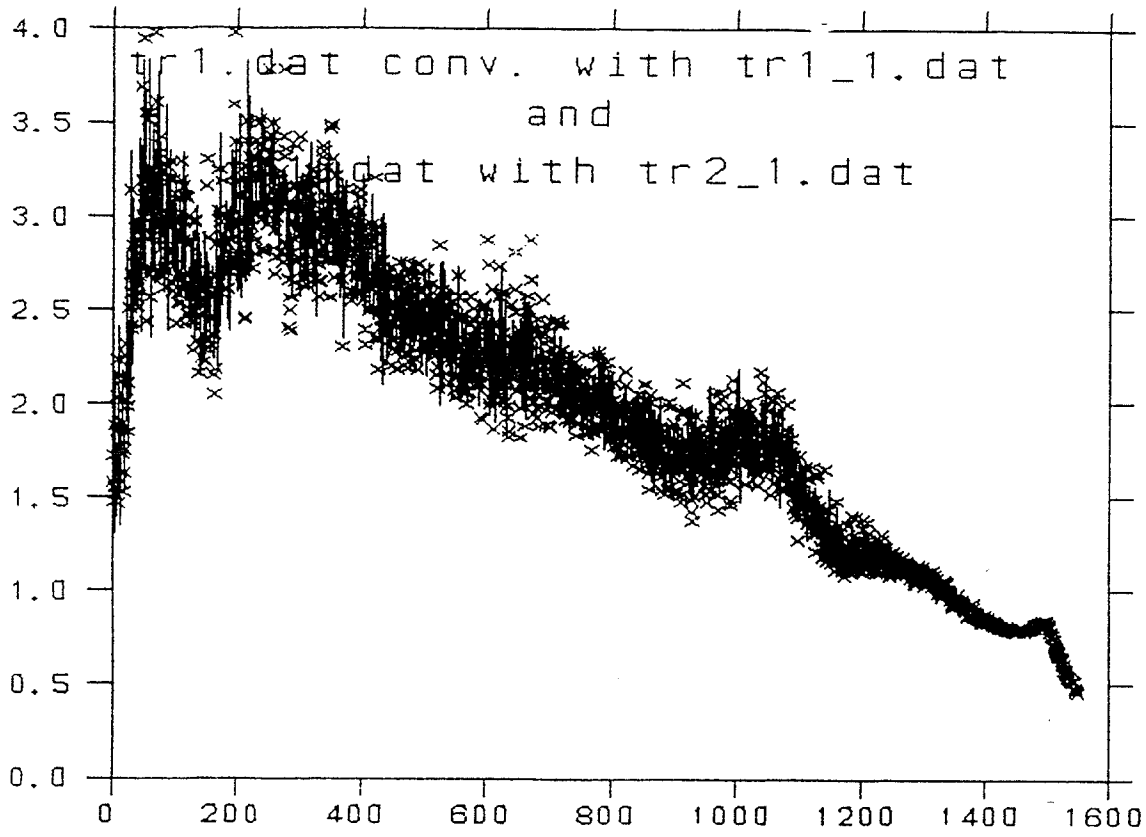

Figure 4.10 : Pre-Breakdown Region signature comparison of Figures 4.8 and 4.9.

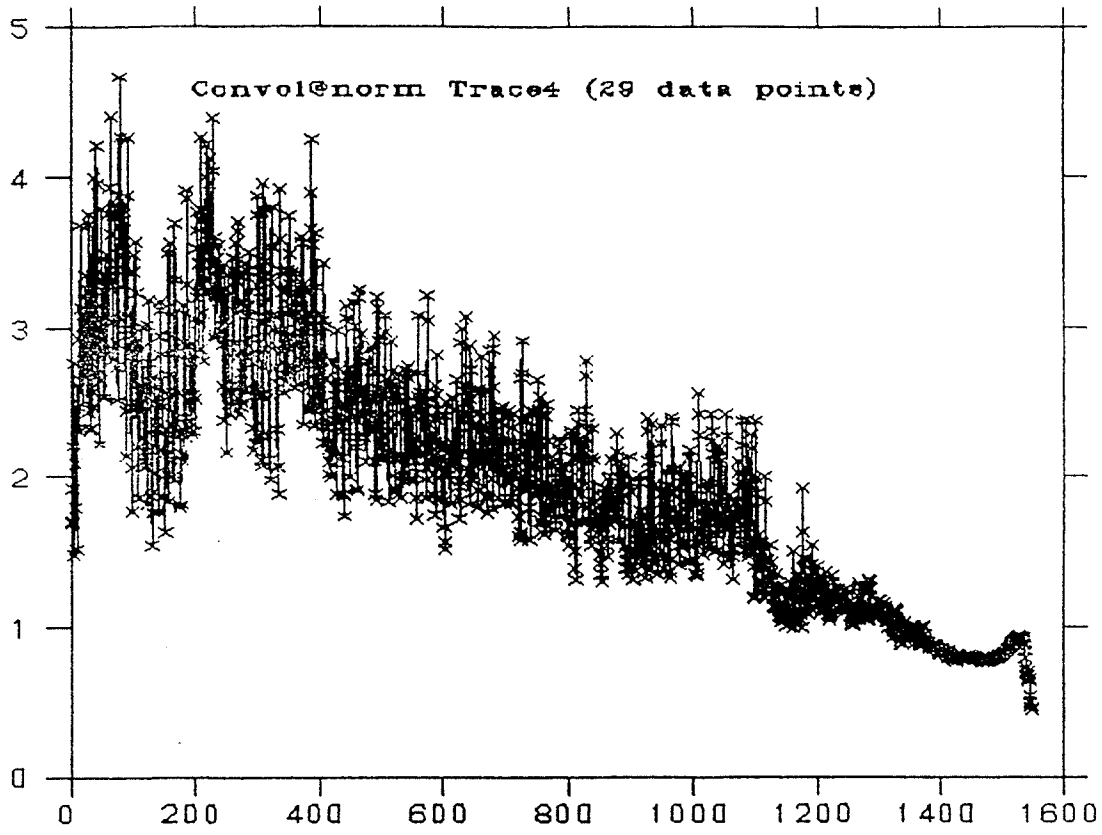

Figure 4.11 : A Pre-Breakdown Region signature using the cCorrelation Procedure Method with 29 data points.

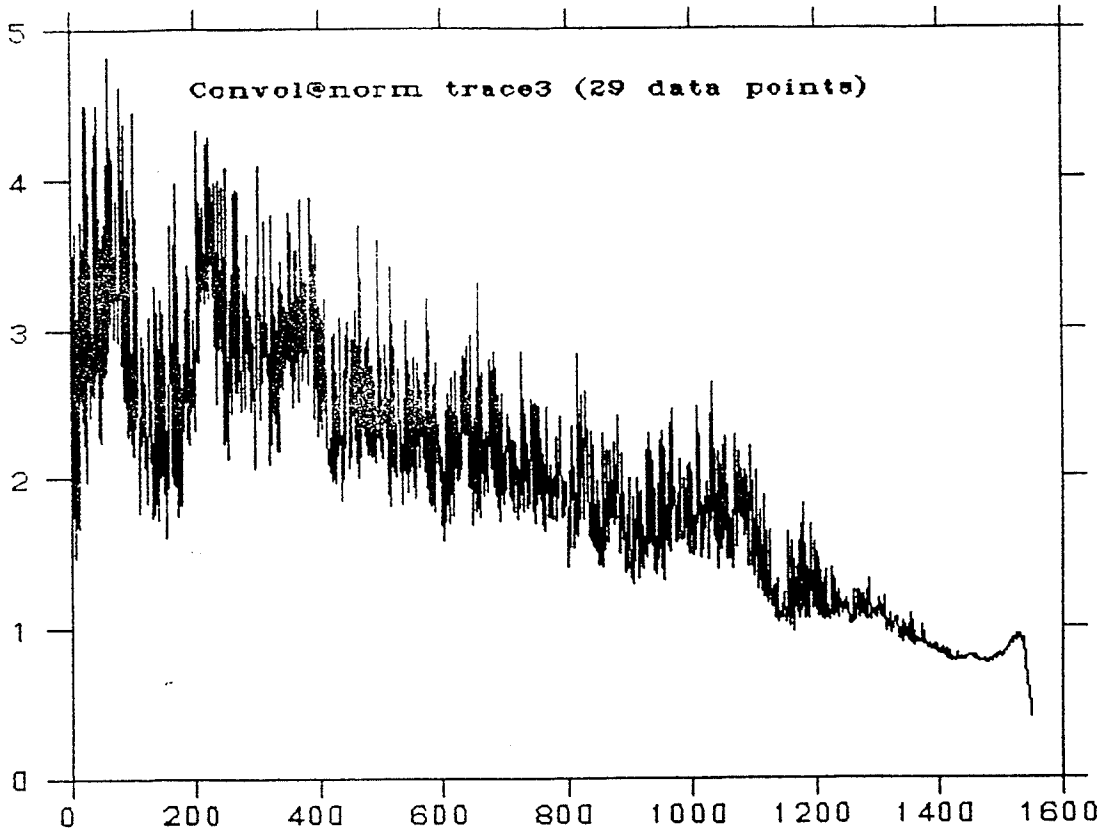

Figure 4.12 : A Pre-Breakdown Region signature using the Correlation Procedure Method with 29 data points.

Experimental results before and after $H^+:H_2^+$ implantation are presented in Figures 4.13 through 4.22. Figure 4.13 shows the spatial dark conduction current. Photoconduction in a tungsten lamp circuit was measured with a neutral density filter, neutral density filter and colored filters as shown in Figures 4.14 to 4.17. Figures 4.18 to 4.22 show the counterparts of Figures 4.13 to 4.17 after hydrogen ion implantation. Figures 4.23 gives a corresponding weight on contact for each datum point taken. The photoconduction experimental set-up was arranged such that a tungsten light source with neutral density filter illuminating the films was placed 100 cm away at an angle of 70 degrees to the normal of the film surfaces. This arrangement was maintained throughout the measurements except that the light intensity was increased after measurement of the implanted film with a neutral density light source. The colour spectrum illuminations were achieved by applying respective coloured filters together with the neutral density light source.

The most obvious difference in conduction current before and after hydrogen ion $H^+:H_2^+$ implantation was that the conduction current increased by a factor of about 25 in the latter case. Photo-to-dark conductivity ratio also increased by a factor of 2.5. One possible explanation is that $H^+:H_2^+$ ions penetrate into those interstitial regions and passivate electrical defects, including dangling bonds. The kinetic energy of $H^+:H_2^+$ ions decreases exponentially on account of the collision cascade and results in broken bonds. It is possible that a number of Si-O bonds have been broken and replaced by Si-H bonds. It is also possible that the energetic ions modify the density distribution of the films on the surface and to a few hundred Å beneath the surface. The overall result is the densification of the films and

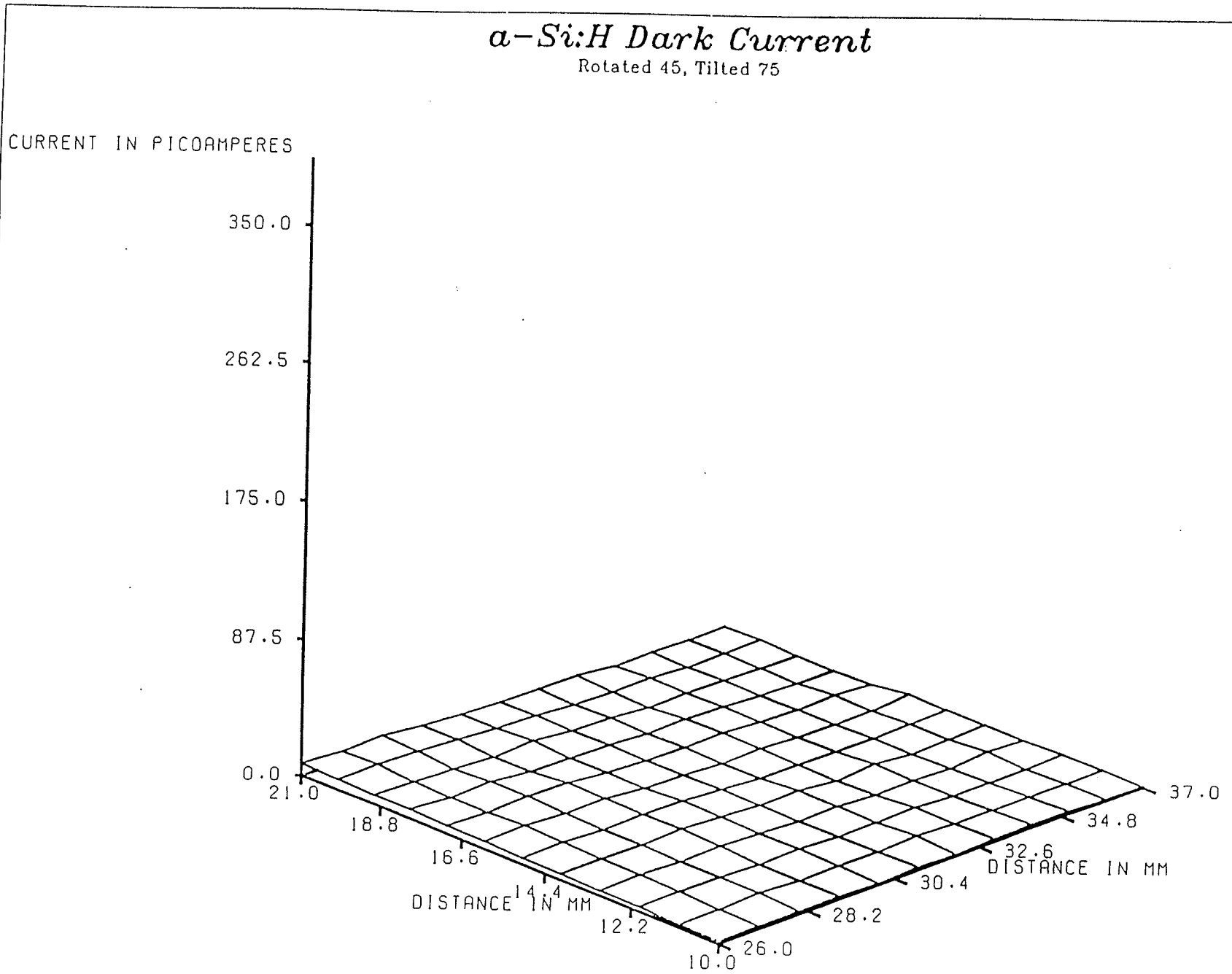

Figure 4.]3 : Spatial dark conduction current before hydrogen ion implantation.

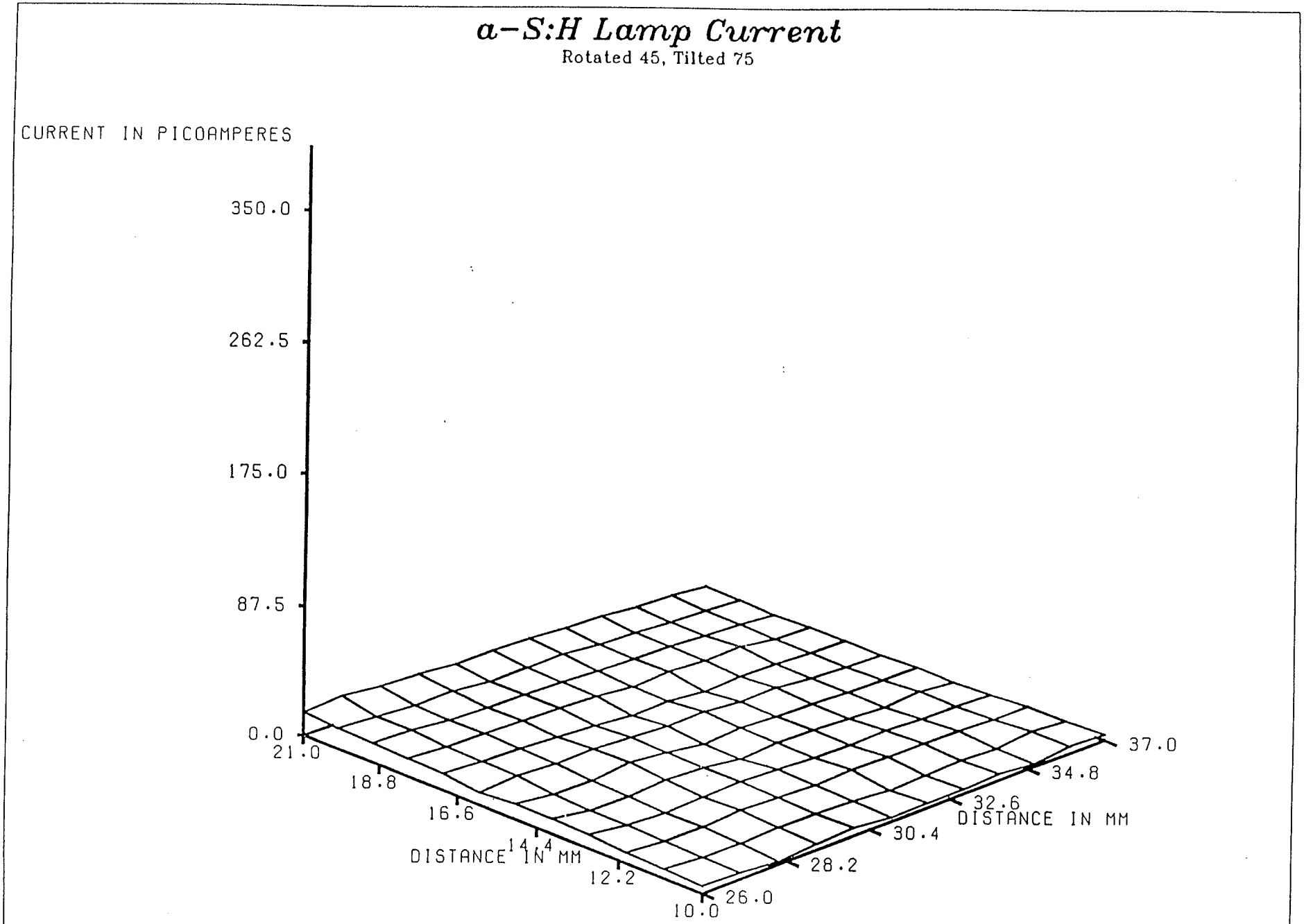

Figure 4.14 : Spatial conduction current before hydrogen ion implantation, using a tungsten light source.

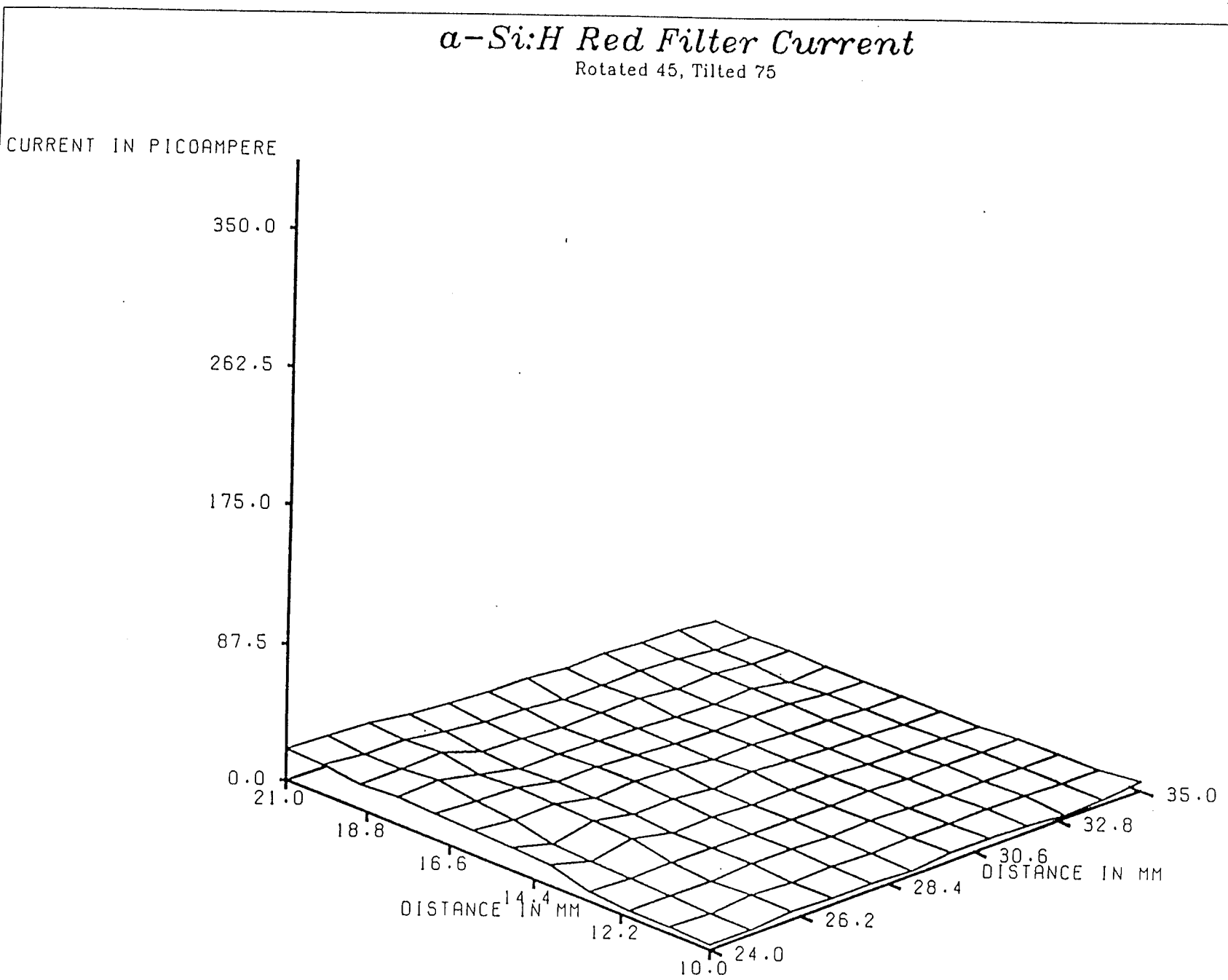

Figure 4.15 : Spatial conduction current before hydrogen ion implantation, using a tungsten light source with a red filter.

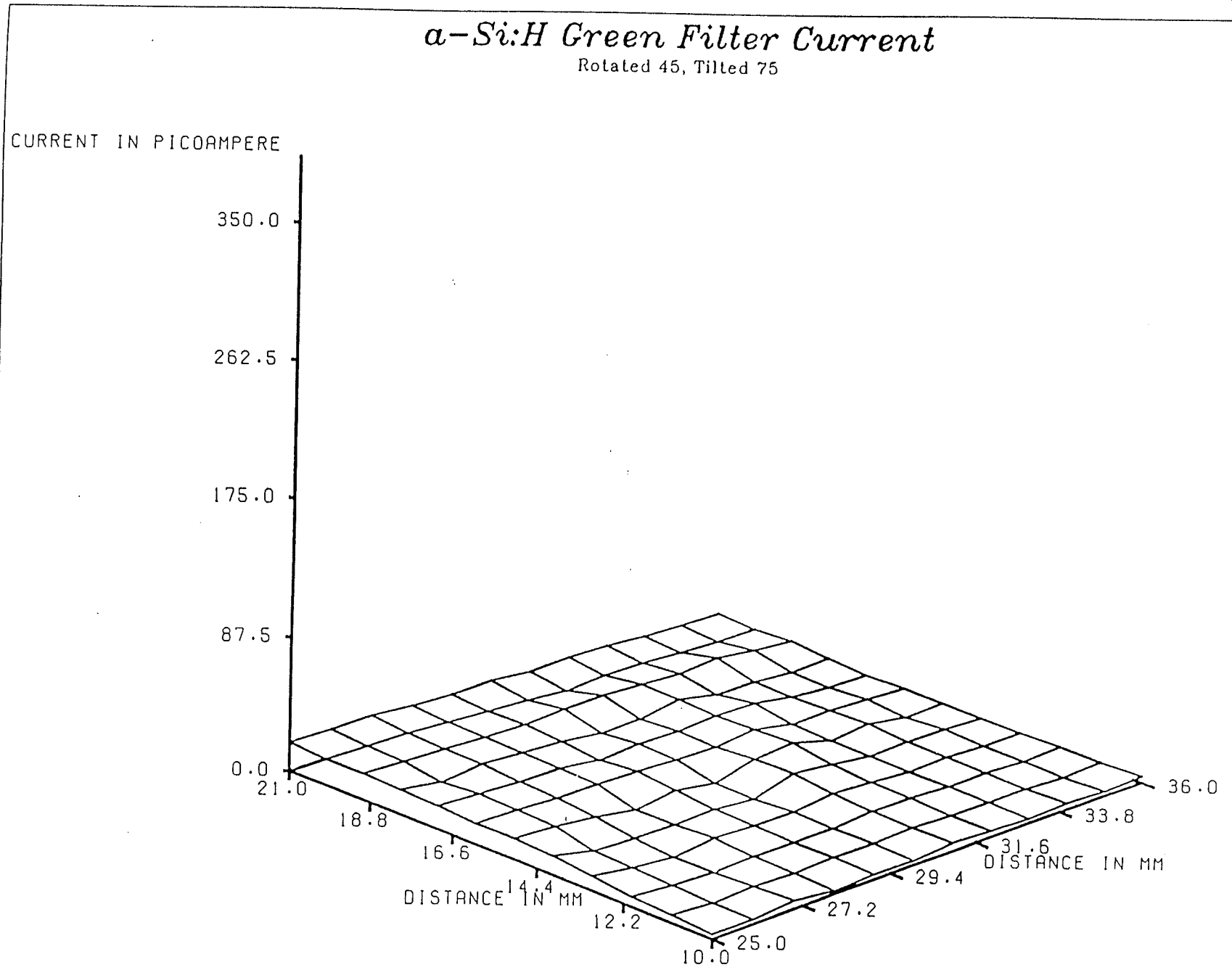

Figure 4.16 : Spatial conduction current before hydrogen ion implantation, using a tungsten light source with a green filter.

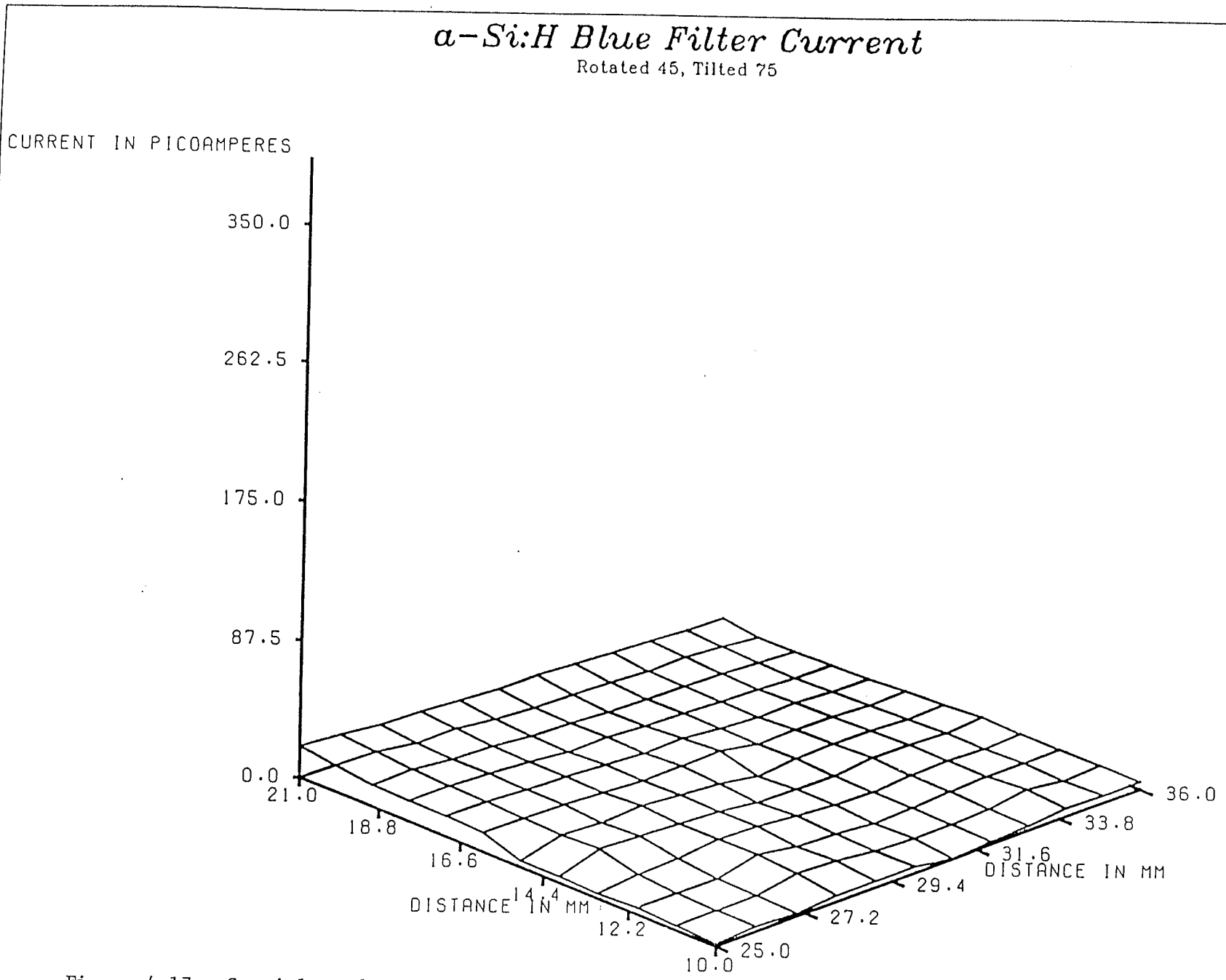

Figure 4.17 : Spatial conduction current before hydrogen ion implantation, using a tungsten light source with a blue filter.

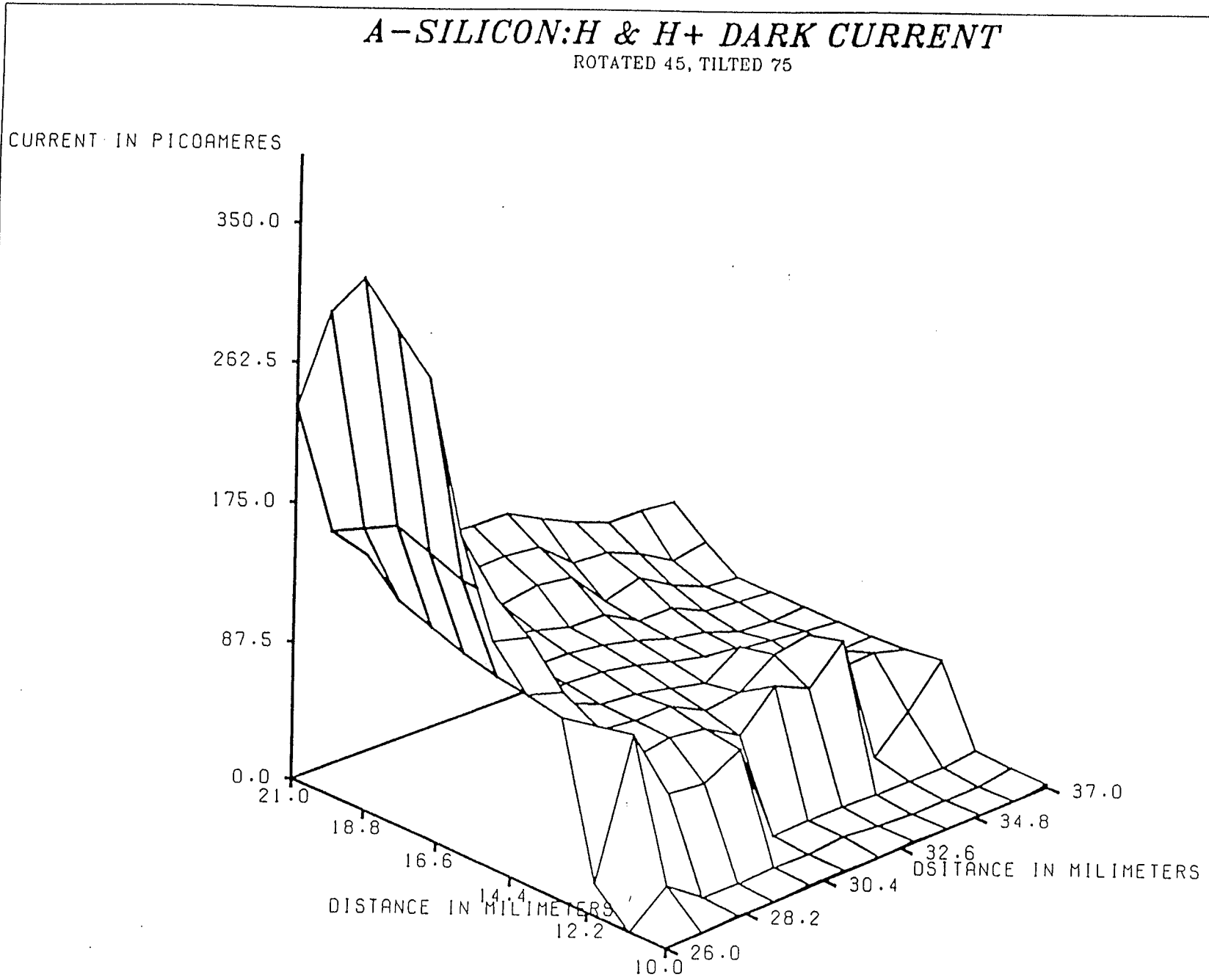

Figure 4.18 : Spatial dark conduction current after hydrogen ion implantation.

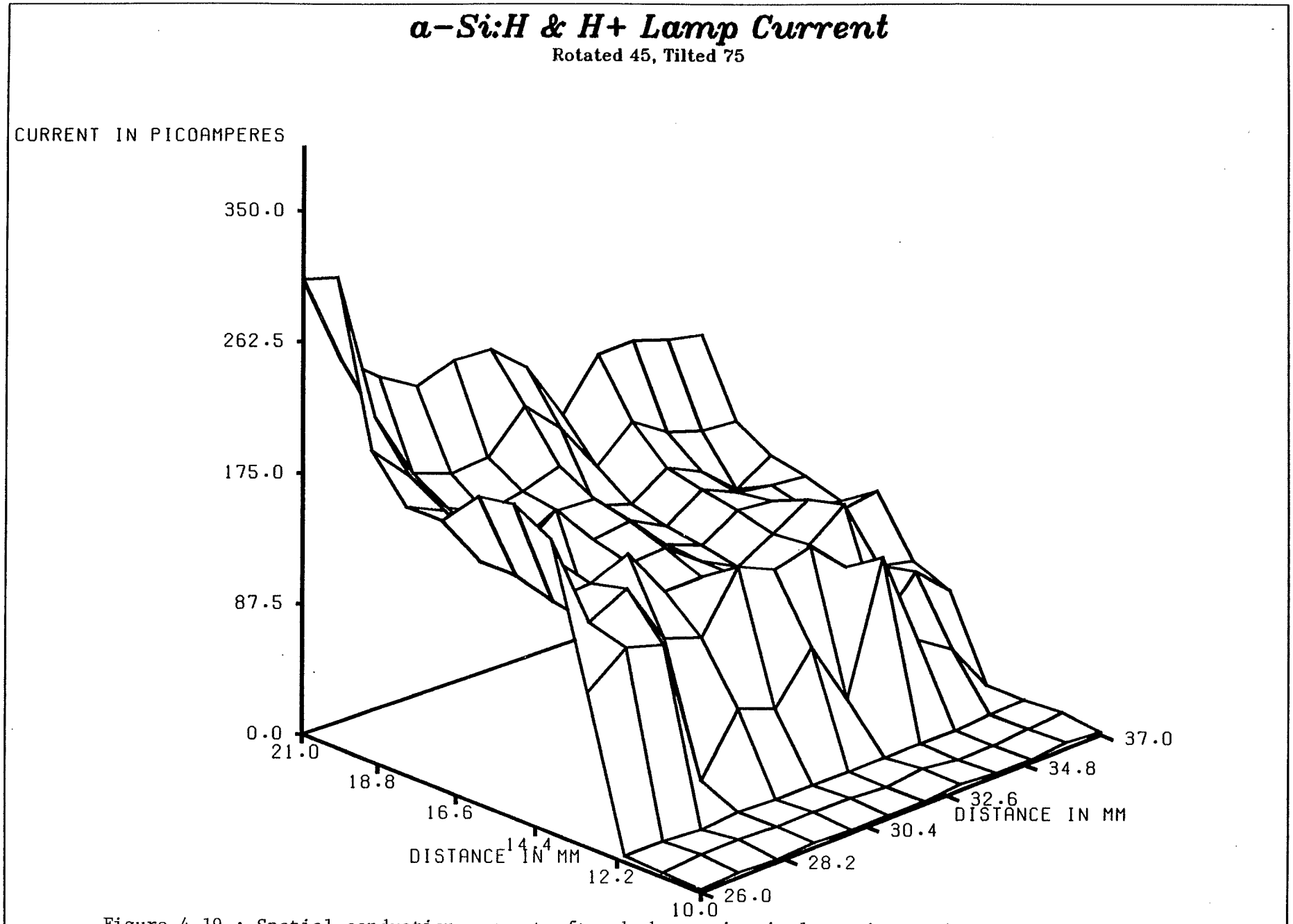

Figure 4.19 : Spatial conduction current after hydrogen ion implantation, using a tungsten light source.

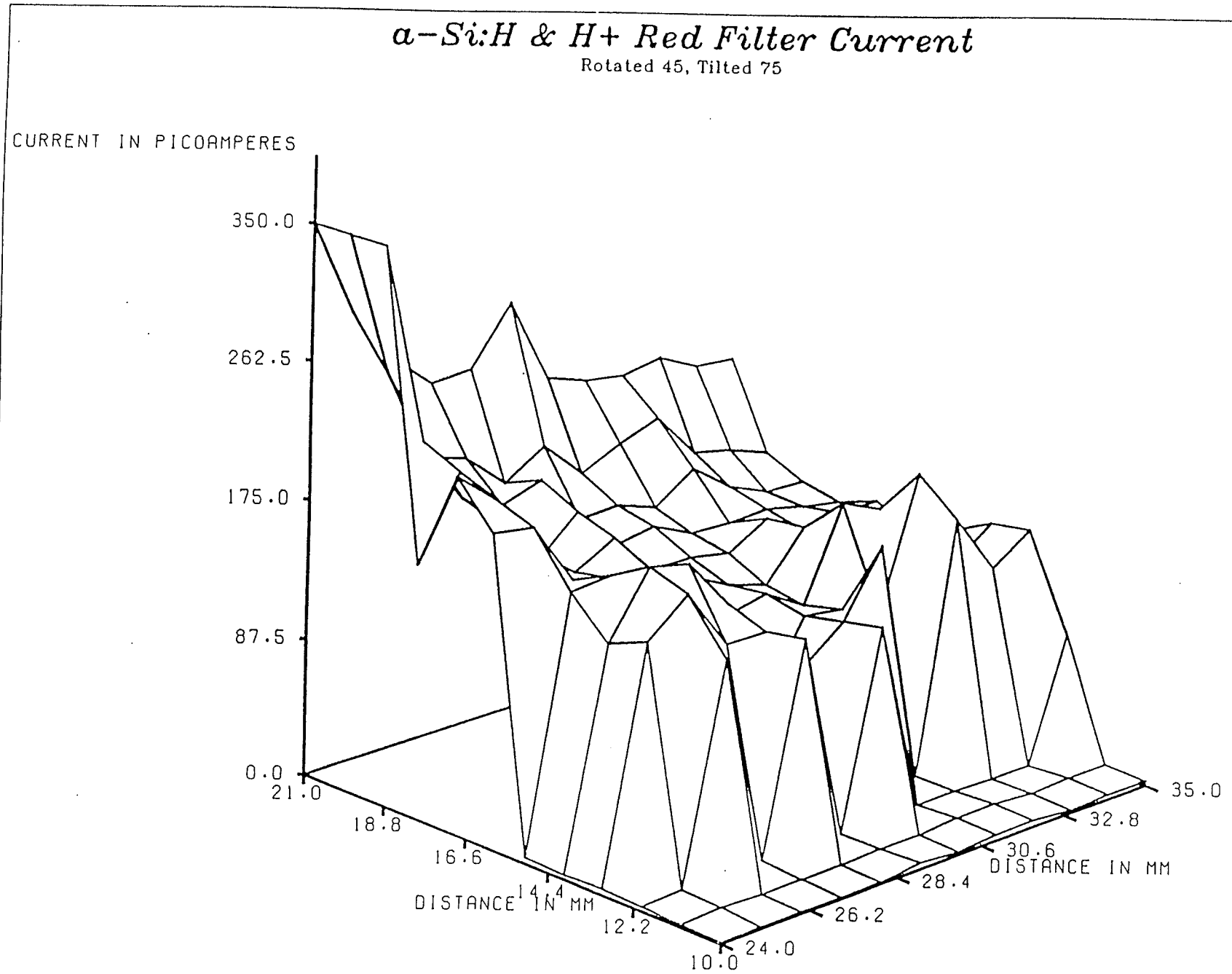

Figure 4.20 : Spatial conduction current after hydrogen ion implantation, using a tungsten light source with a red filter.

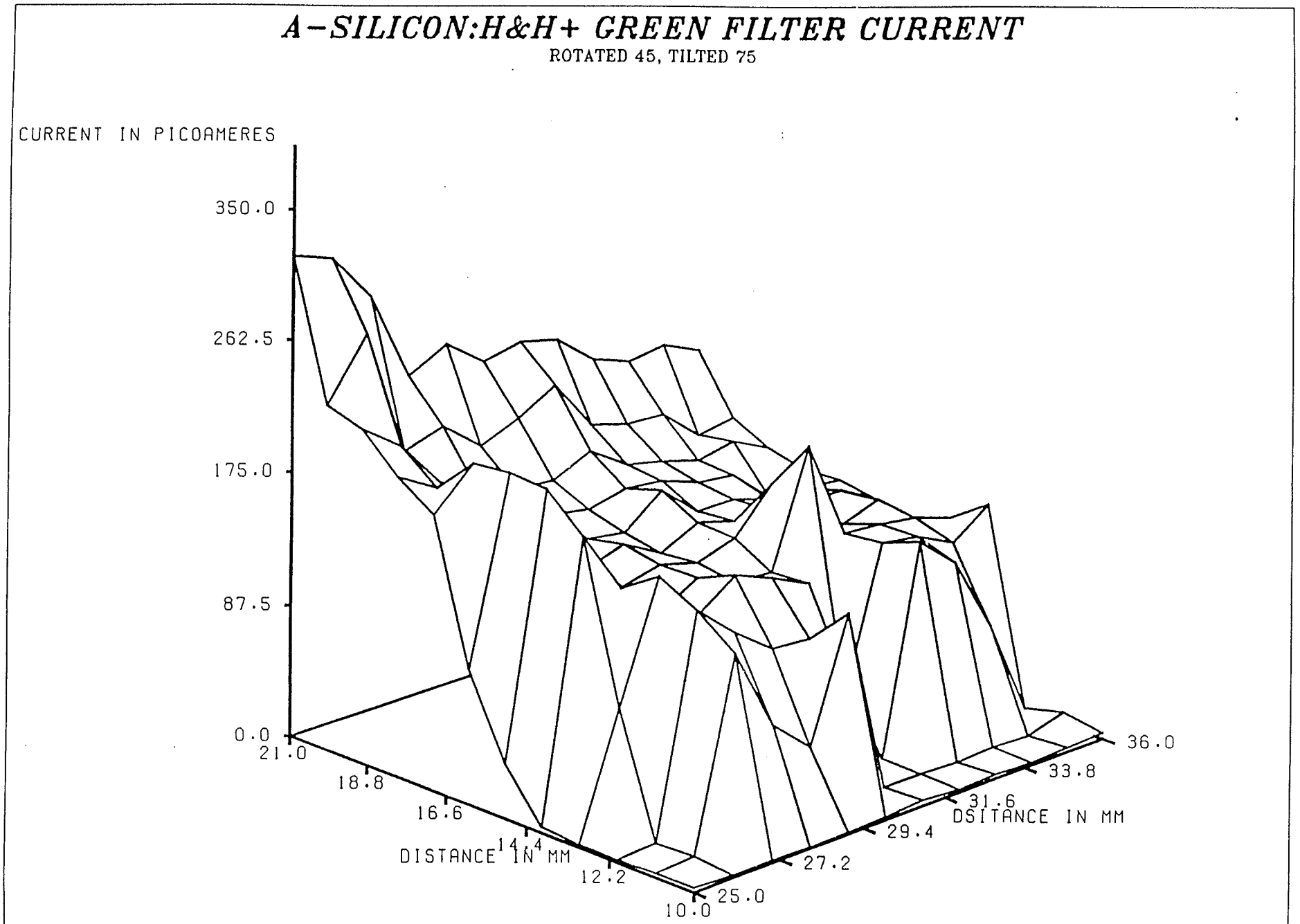

Figure 4.21 : Spatial conduction current after hydrogen ion implantation, using a tungsten light source with a green filter.

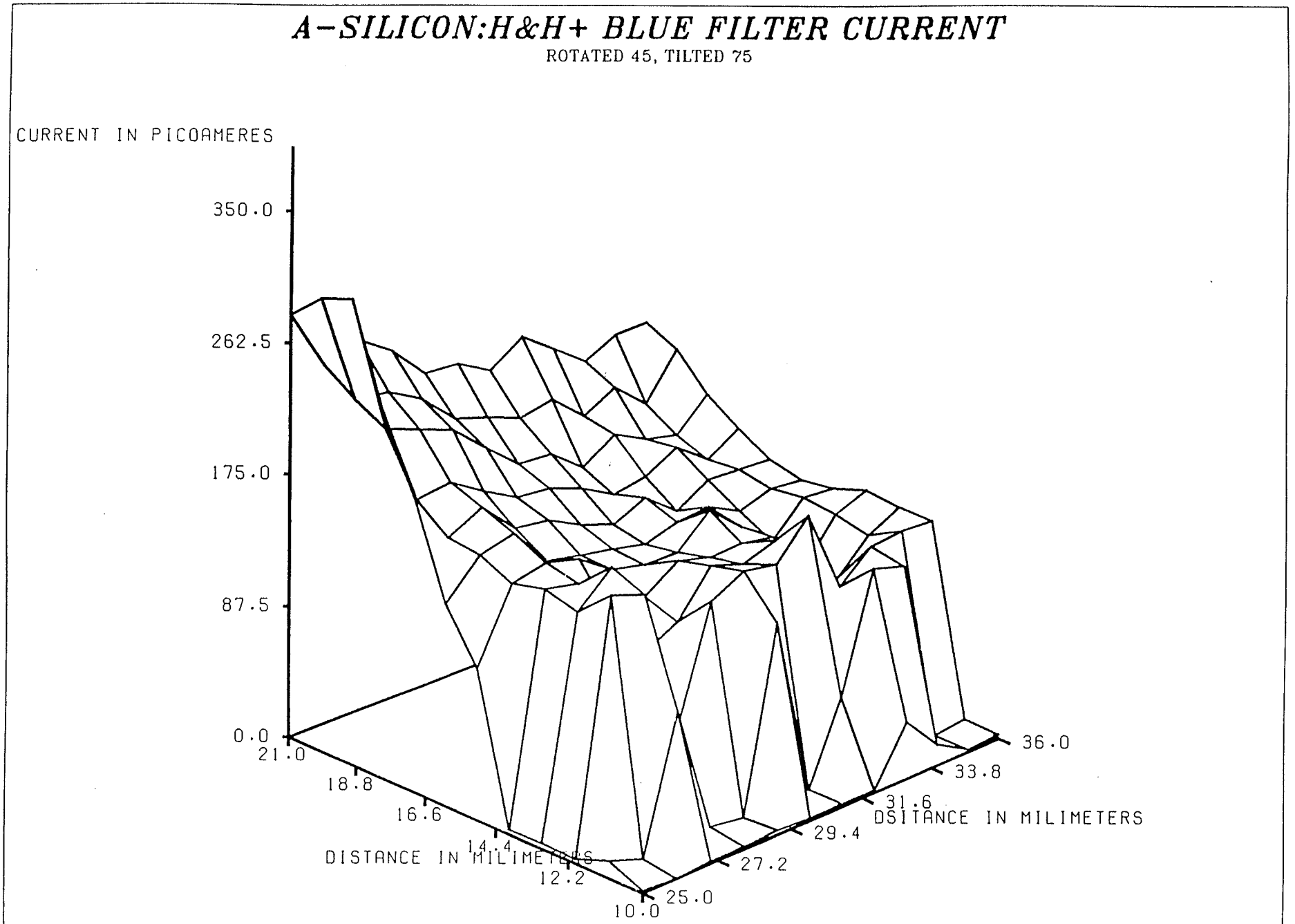

Figure 4.22 : Spatial conduction curren after hydrogen ion implantation, using a tungsten light source with a blue filter.

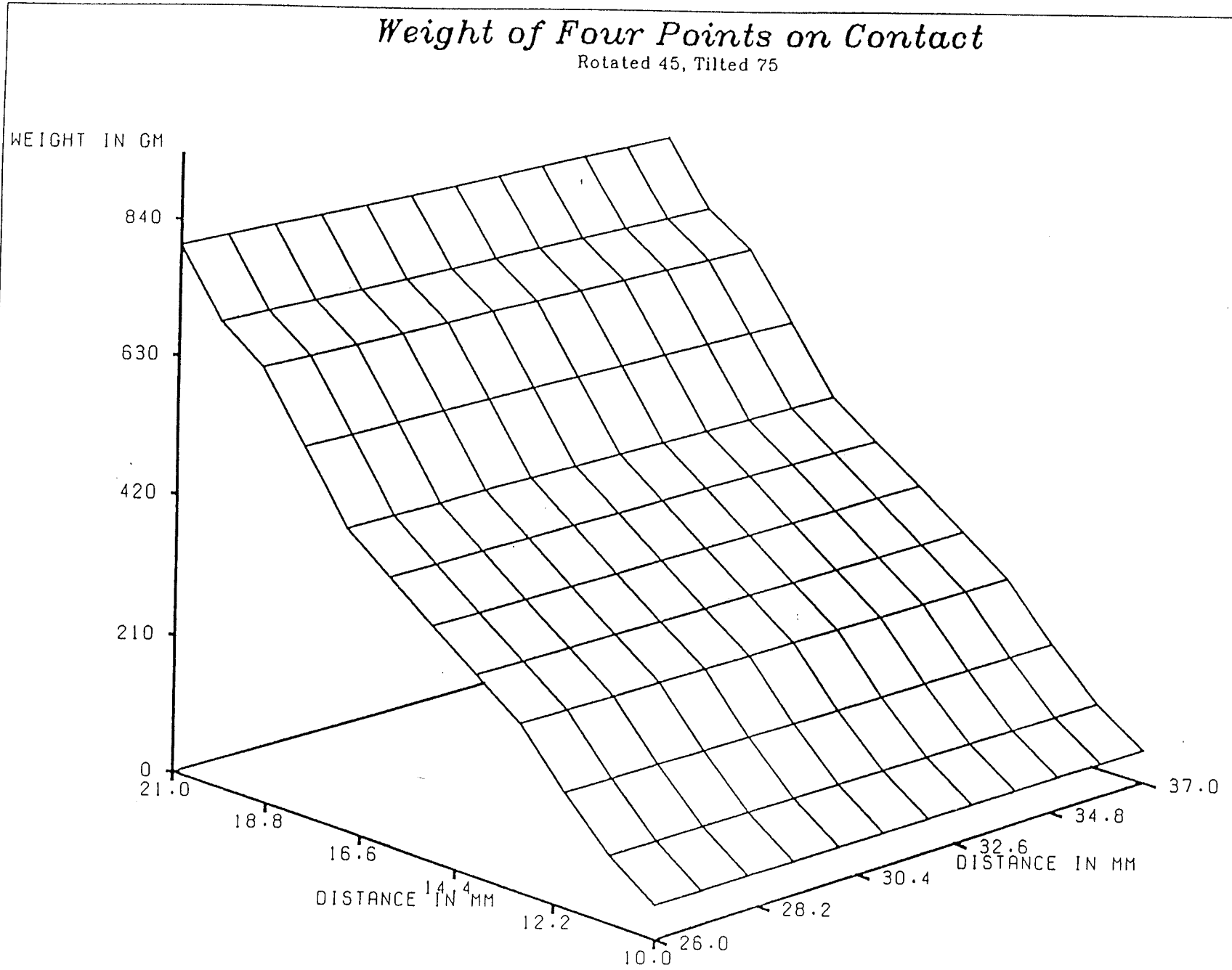

Figure 4.23 : Weight of four points on contact for all the data points taken.

intensification of the hydrogen concentration. These effects are constructive. Damage to the implanted film surface is demonstrated by the extremely low conduction current (e.g. close to background current) when the weight of the four points in contact is less than 170 gm. A leap in conduction current from background value to a value about 25 times bigger than unimplanted films occurs when the weight of the four points in contact exceeds 170 gm. A possible explanation of such a phenomenon is that when contact weight is greater than 170 gm, the four points penetrate the damaged surface and make contact with the improved region of the film, resulting in higher conduction currents. Such an explanation, if true, indicates that a certain degree of penetration of hydrogen into interstitial regions of the a-Si:H film causing physical and chemical interactions can indeed occur. Another observation is that before H^+:H_2^+ implantation, the red filter conductivity is proportionately higher than for the green filter, which in turn is higher than for the blue filter. After hydrogen ion implantation, green and blue filter conduction currents improve in comparison to the corresponding red filter. Therefore, a shift in photoconductivity from the red light spectrum to a more energetic green and blue light spectrum occurs. Before H^+:H_2^+ implantation, the red spectrum current is about 10 % less then that due to the tungsten neutral density light source, whereas for the blue light spectrum photoconduction current is about 30 % less. For the green light spectrum the photoconduction is somewhere in between. After H^+:H_2^+ implantation, all photoconduction current measurements are within 10 % of each other. There is no valid explanation for such a phenomenon except that the light spectra other than the red have been modified while passing through the damaged

surface layer into the H enhanced interior. The damaged surface may have acted as a red light filter, for the film itself is reddish in colour.

4.3 : A New Technique of Metal Contact Fabrication

Figure 4.24 shows a SEM photograph of the Si surface with a conductive region of silver introduced by means of 80 - 100 keV H^+:H_2^+ ion bombardment. The silver film deposited by the process outlined here is fairly uniform and is between 0.6 and 0.7 μm thick. The out-diffusion of H^+:H_2^+ ions trapped between the silver layer and the silicon is prevented because of the high Z value of silver, and results in the formation of bubbles. The proper negative biasing and heating of the Semiconductor helps in the out-diffusion of H_2, thus reducing the density of bubbles on the deposited silver surface. In order to investigate the presence of silver below the surface, the silver was removed from the surface of the semiconductor. The semiconductor wafer without any Ag on its surface was analysed by the PIXE technique described earlier. The K x-ray spectrum at an incident proton energy of 40 MeV is given in Figure 4.25b. For comparison, the K x-ray spectrum of an alloy of silver and gold was also obtained at an incident proton energy of 40 MeV and the corresponding Kα and Kβ peaks for silver are shown in Figure 4.25a. This confirms the localised presence of pure silver in the bulk of silicon wafer.

4.4 : Plasma Interaction and Ion Implantation of Refractory material

The XPS data from the surface of the TiC(PS) coating from inside the Tokamak

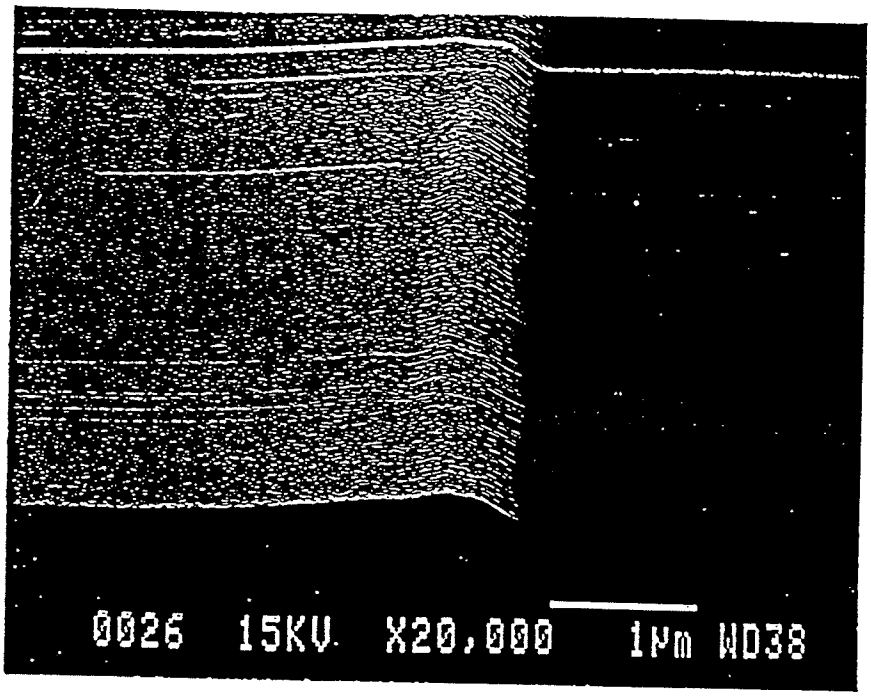

Figure 4.24 : Scanning electron micrograph of a 0.3 µm thick silver layer formed on silicon wafer.

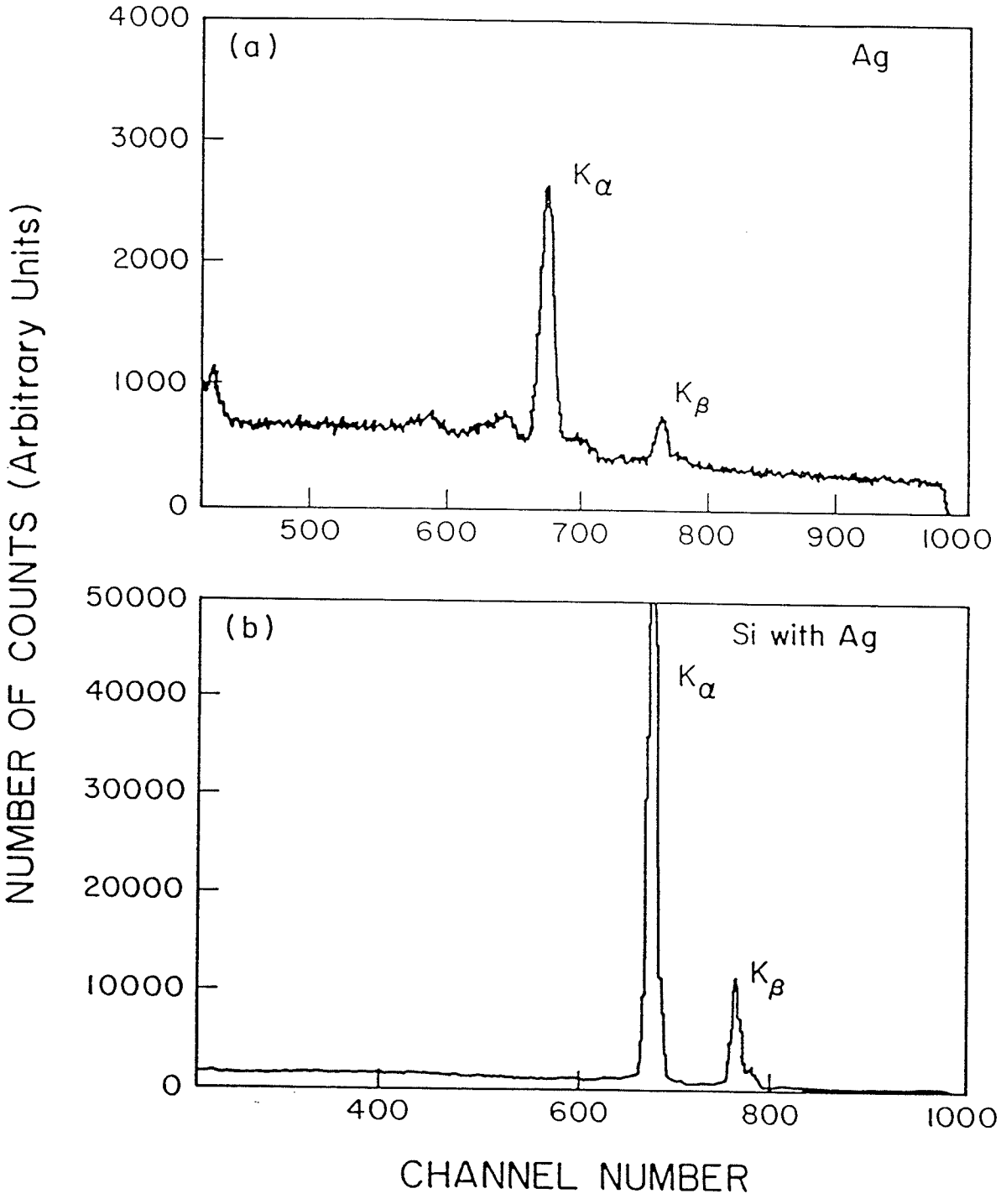

Figure 4.25 : X-ray spectra from the PIXE analysis at 40 MeV incident proton energy: (a) K x-rays from a Ag-Au alloy and (b) K x-rays from the silicon/silver target of the present study. The channel numbers and counts are proportional to the energies and the number of x-rays detected respectively.

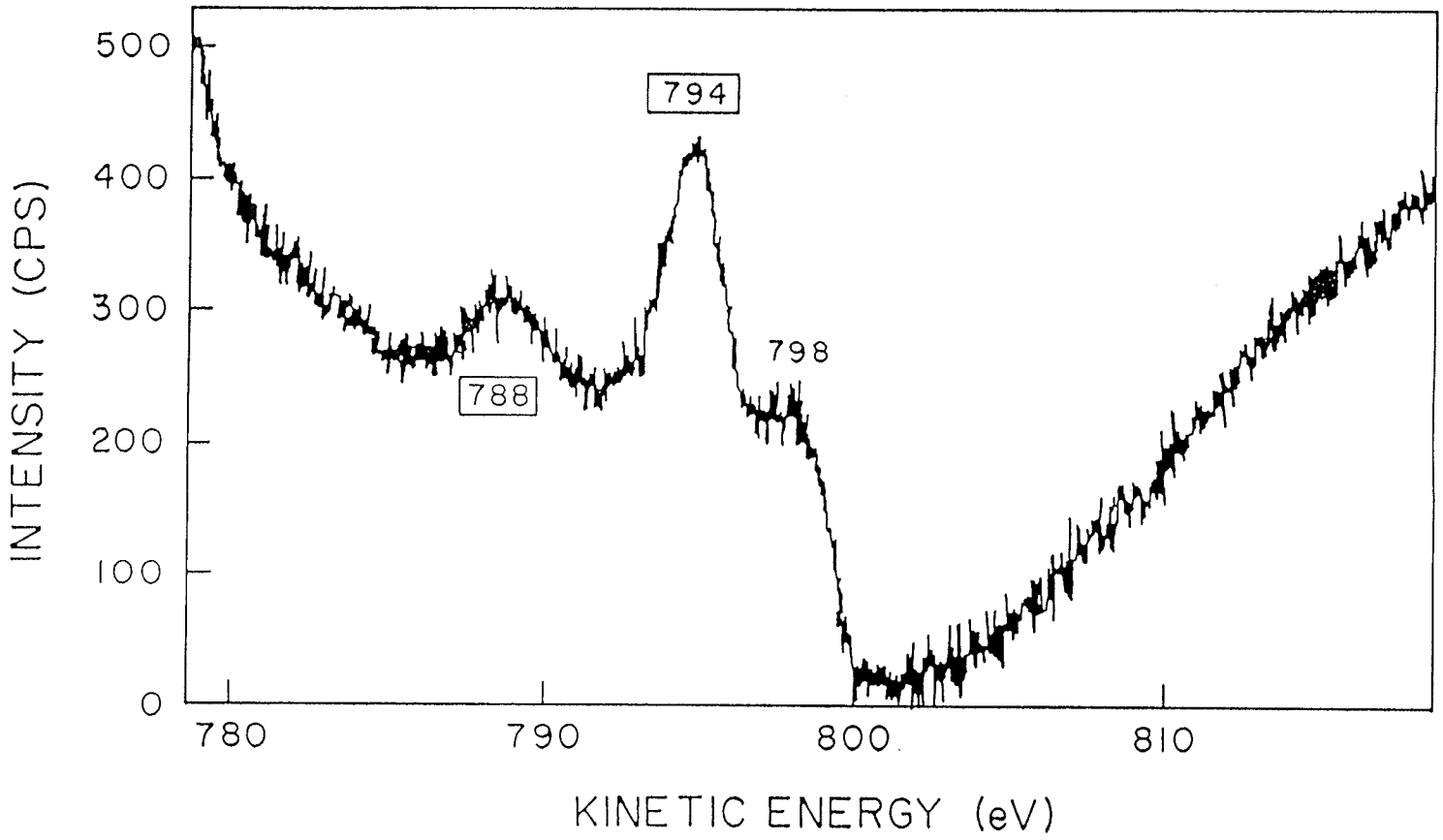

Figure 4.26 : XPS spectra of TiC(PS) coating subjected to ≃ 1500 plasma discharges inside the Tokamak fusion reactor. Intensity (CPS) vs. Kinetic Energy (ev).

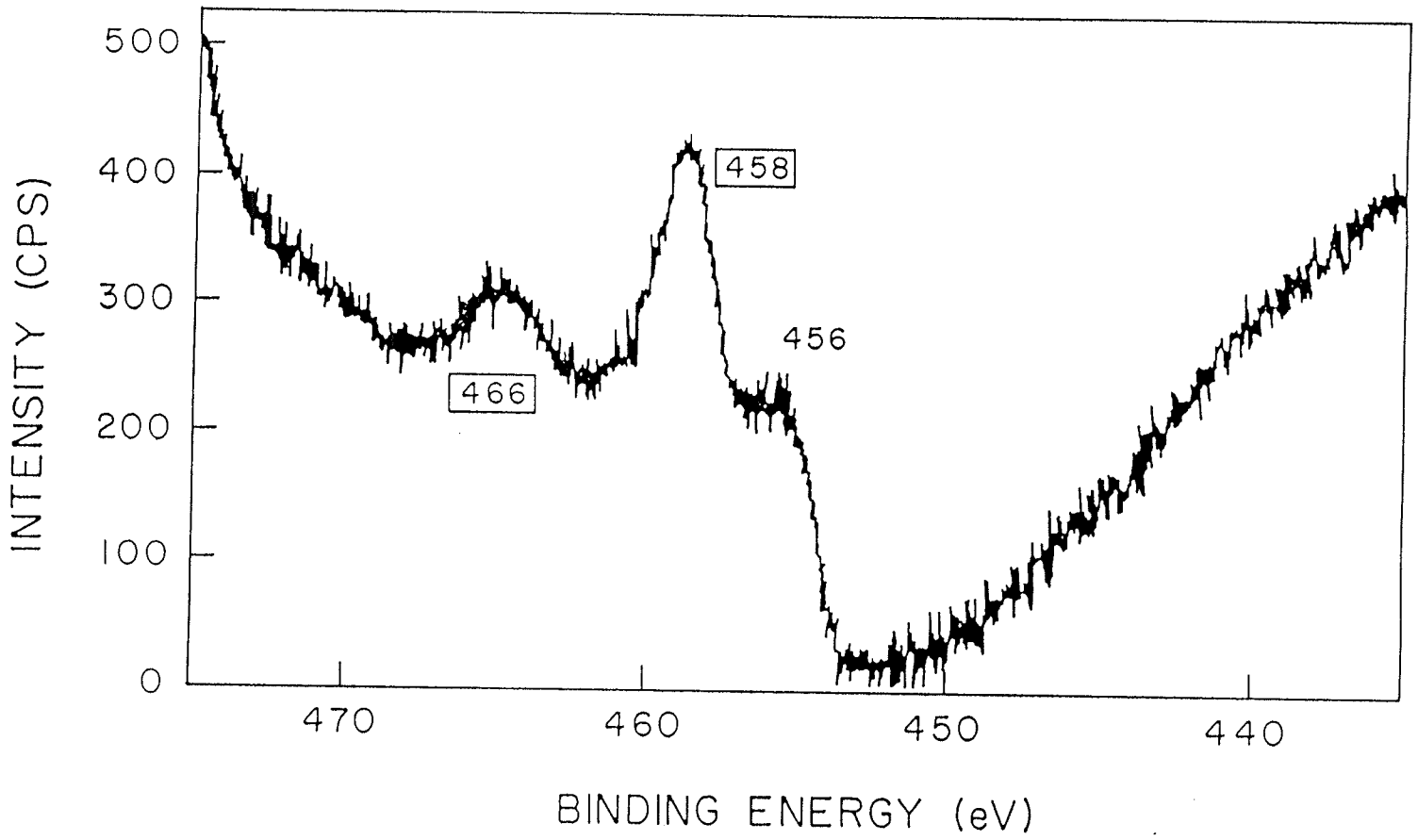

Figure 4.27 : XPS spectra of TiC(PS) coating subjected to ≃ 1500 plasma discharges inside the Tokamak fusion reactor. Intensity (CPS) vs. Binding Energy (ev).

reactor are given in Figures 4.26 and 4.27. The kinetic energy (eV) vs. intensity (counts/sec) data of Figure 4.26 reveal a titanium $^2P_{3/2}$ line at 794 (eV). Theoretically this line should be much stronger and should have a value of 799 (eV). Because of the chemical and charge shifts the 799 (eV) line however is shifted down to 794 (eV). The 798 (eV) line is probably an Auger line or an artifact associated with the XPS shake-up-line. The binding energy (eV) vs. intensity (counts/sce.) data of Figure 4.27 have a strong line at 458 (eV). This is the 455 (eV) line shifted up in terms of binding energy due to chemical and charge shifts. The 457 (eV) line can probably be associated with the XPS (shake up line). These data confirm the presence of free Ti on the surface of the TiC(PS) coatings which have been subjected to plasma ion bombardment. The argument as to whether this is due to carbon deficicency in the coating [for coatings are somewhat porous and are carbon deficient, $(C/Ti = 0.74-0.84)$ depends on spraying conditions and this fact can play a role in the hydride formation and blistering], or to the dissociation of TiC molecules subjected to ions from the plasma, still needs to be resolved. If there were free Ti atoms available to the impinging hydrogen ions, titanium hydride could be formed. Since the implanted coating is showing the presence of free Ti atoms, the likelihood of TiC molecule dissociation when subjected to H ions is very real. The dissociated carbon atoms can combine with hydrogen to form carbon hydrogen complexes and some titanium hydrogen complex formation is also expected. For this to be verified, the coating surface was analysed by the surface Raman scattering technique, and the observations are compared with those of H^+:H_2^+ implanted TiC wafer. The Inelastic Light Scattering data of TiC wafers are shown in Figure 4.28, and Figure

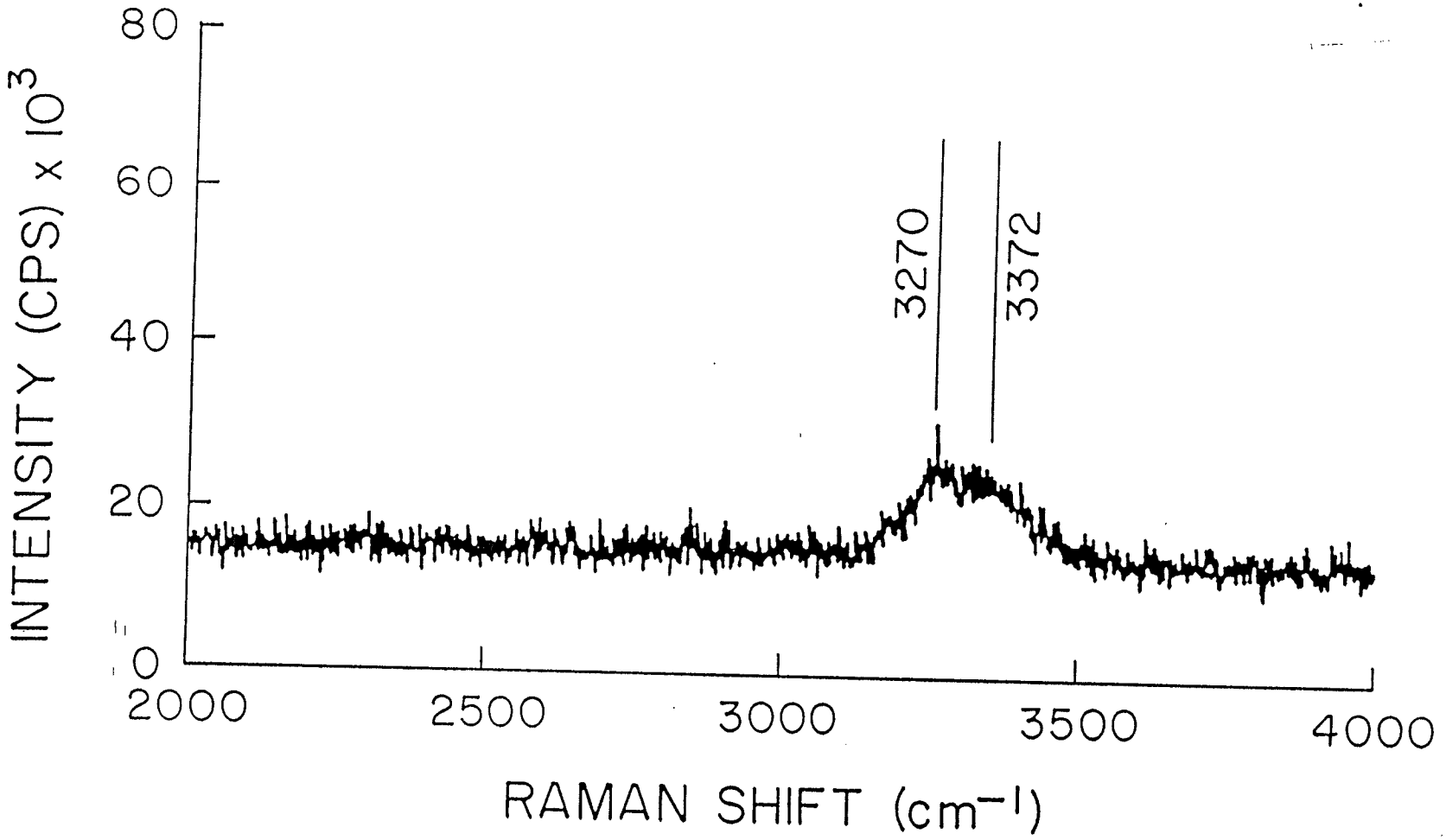

Figure 4.28 : Raman spectrum of the 60 Kev H_2^+ bombarded surface of TiC. Laser power 500 mw. Entrance slit-80 μ. Total data acquisition time - 6 hours. (multiple scans with 2 s/step.)

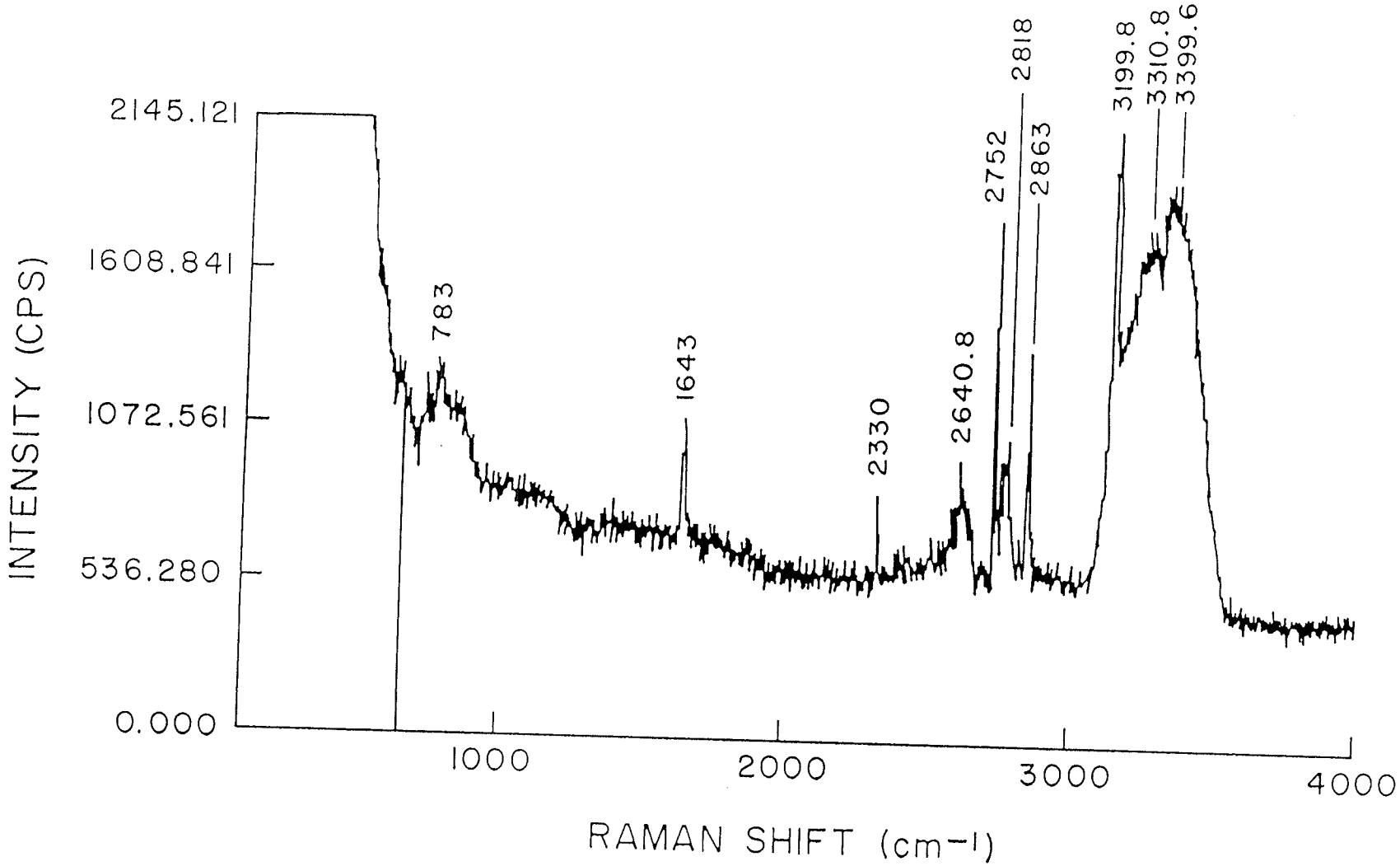

Figure 4.29 : Raman spectra of the TiC(PS) coating surface subjected to ≃ 1500 plasma discharges inside the Tokamak fusion reactor. Raman shift (cm^{-1}) vs. Intensity (CPS).

4.29 shows the data for TiC (PS) for comparison. The Raman scattered signal of Figure 4.28 is accumulated over a period of 6 hours from the TiC wafer bombarded with 60 keV H^+:H_2^+ to a fluence of 10^{17} ions/cm^2. A doublet with component Raman bands at 3270 and 3372 cm^{-1} is observed in the Raman spectrum. Gaseous methane CH_4) has been studied (30,31) extensively and the Raman spectrum is known to contain two active fundementals at 2914.2 and 3022.0 cm^{-1} respectively. Dension (32) also calculated the first order frequencies from the observed fundamentals. He obtained for CH_4 (in cm^{-1}) $w_1 = 3029.8$ and $w_3 = 3156.9$ respectively. The Raman bands observed by us have slightly higher shifts than the Raman bands of pure CH_4 gas. It is likely that in our situation some impedence is offered to the CH_4 moleccules in their vibration, and this in turn can result in dampening of the vibrational frequencies.

The Inelastic Light Scattering data of TiC (PS) in Figure 4.29 contains Raman active bands at 783, 1642, 2330, 2640.8, 2752, 2818, 2863, 3199.8, 3310.8 and 3399.6 cm^{-1}. Molecules containing C-H bond have normal frequencies of about 3300 and 700 cm^{-1}, for example in C_2H_2 molecules these fundamentals have been reported at 3377 cm^{-1} (Raman) and 729 cm^{-1} (infrared) respectively (33). The 3399.6 cm^{-1} Raman band in our observation can thus be attributed to the C-H stretching vibration of C_2H_2 molecule. The 3199.8 and 3310.8 cm^{-1} band are the corresponding bands in Raman spectrum of the wafer. This comparison indicates that the bombardment of the TiC coated surface with energetic H ions from the fusion plasma results in the decomposition of TiC molecules into Ti and C atoms. The free carbon combines with available impinging hydrogen ions and results in

the formation of methane and acetylene CH_4 and C_2H_2. The formed gases get absorbed on the TiC surfacce. The C=C and C-C stretching vibrations for the hydrogen and carbon complexes occcur at $\approx$ 1600 and 2300 cm^{-1} respectively (34). The weak 1643 and 2330 cm^{-1} Raman bands in our study can be attributed to such vibrations. The presence of these bands in the observed Raman spectrum of the implanted TiC(PS) coating surface suggests the formation and absorption of carbon and hydrogen complexes. The Ti from the decomposed TiC molecule must be present on the surface of TiC(PS) coating and its presence is confirmed by the XPS data as discussed earlier. However, some of the free Ti atoms on the surface can combine with impinging hydrogen ions to form hydrides. The 783 cm^{-1} broad Raman band can be understood in terms of titanium hydrogen stretching (35). The broad and weak 2641 cm^{-1} band in our observation can be interpreted in similar fashion in terms of linear Ti-H stretcching (35,36). The 2752, 2818 and the 2863 cm^{-1} bands in our observation can be attributed to the various CH stretchings of the C_2H_6 molecule, which for pure C_2H_6 gas appear at 2744, 2778, 2839.5 and 2963 cm^{-1}.

Chapter 5 : CONCLUSIONS

5.1 : Conclusions and Suggestions for Future Research on Implantation Study of Dielectrics

5.1.a : Conclusions

The study undertaken here concludes that H^+:H_2^+ ion implantation results in the surface breakdown of the dielectric 'ISP'. Furthermore, from the fact that ion implantation breaks many bonds, we attribute the main cause of H^+:H_2^+ ion implantation induced surface breakdown to the fragmentation of the long chain molecules on the surface (and a few thousands of Åbeneath the surface) of the dielectric 'ISP'. The H^+:H_2^+ ions in their journey through the dielectric 'ISP' undergo a cascade of collisions (48,49). In the collision process, the H^+:H_2^+ ions combine with the surface molecules of the dielectric 'ISP' to form totally different molecules and cause dissociation of macromolecular chain into various segments. These segments might possess polar behaviour thereby affecting the dielectric constant of the material. These conclusions are strongly supported by the Raman light scattering analysis. The surface breakdown might be avoided by exposing the dielectric 'ISP' surface to energetic N_2^+ ions prior to H^+:H_2^+ implantation. It is well known that N_2^+ implantation of steel, nickel and many other metals hardens the metals against degradation, improves adhesive energy (37), wear (38-44) and fatigue (38,44-46), but the possibility of hardening dielectrics with the N_2^+ implantation needs to be verified. However, the nitrides are known for their surfaces hardness and insulating

behaviour. Therefore, the successful hardening of the solid dielectric surfaces using N_2^+ implantation technique is worthy of attention.

It is well known that ion implantation of a material causes surface modification of the material, but the diffusion process and the consequent effect of ions inside the material is difficult to assess. However, from the results of bulk thermal breakdown experiments for the unimplanted, implanted and electron irradiated dielectric 'ISP', one can safely say that H^+:H_2^+ implantation does little to modify the bulk electrical and thermal properties of the dielectric 'ISP'.

Low energy electron bombardment also does little to affect the dielectric 'ISP' both on the surface as well as beneath the surface, but the effects of higher energy electron bombardment are unknown. The search to understand the effects of high energy electron irradiation is underway with electron energies ranging from 5 - 25 keV generated by SEM (Scanning Electron Microscopy).

An important finding from this study is the discovery of a characteristic behaviour occuring prior to the actual bulk dielectric thermal breakdown (the 'P.B.R.'). The ability to recognise the dielectric in such a situation in the shortest time possible is crucial to the prevention of thermal breakdown. This study shows three methods to recognise the 'P.B.R.' automatically using a mini-computer (the VAX/750). Among the three alogrithms, the 'C.P.' developed for the study generated a distinct signature for the dielectric 'ISP' in this 'P.B.R.'. The application of the 'C.P.' technique is demonstrated to be critical to the prevention of thermal breakdowns in the laboratory simulation.

5.1.b : Suggestions for Future Research

Low energy electron ($\leq$ 720 eV) irradiation of dielectric 'ISP' has been investigated in detail and the results show no detectable effect on and below the surface of the dielectric ISP. However, in a high power system, electrons of energy much greater than 720 eV are generated. Energetic electon bombardment of solid organic dielectrics might cause dissociation of macromolecular chain into fragments. These fragments can have different dielectric constants. Therefore, the investigation of high energy (5-25 keV) electron irradiation of solid organic dielectrics similar to the dielectric 'ISP' is being undertaken using a SEM, (SEM is used for its high vacuum, well defined fluence and variable electron energy).

We have shown that the bulk thermal breakdown behaviour of the dielectric 'ISP' at constant applied voltage can be divided into four regions (i.e. N.A.R., P.B.R., T.R. and B.R.). The T.R. contains all the indications about the breakdown which is sure to occur if sufficient time is allowed. Detailed investigations are needed to understand the physical state of the dielectric 'ISP' in this region. We would like to continue this investigation using Fast Fourier Transform , Power System Analysis, the Maximum Entropy Method and the Maximum Likelihood Method data processing procedures to determine the actual electrical and thermal state of the dielectric in this region. We have speculated that solid organic dielectrics will have similar behaviour to the behaviour observed in the study of dielectric 'ISP' and therefore recommend to undertake similar testings for the other solid organic dielectrics frequently used in high power systems, in order that the breakdown prevention techniques developed in this study can be applied to a wide range of power system analysis.

We have concluded that the H^+:H_2^+ ions in their journey through the dielectric 'ISP' combine with surface molecules, forming totally new molecules or complexes and cause dissociation of the macromolecular chain into various segments (refer also to 47). These species can possess polar behaviour thereby affecting the dielectric constant of the 'ISP'. In order to reduce the reactivity of the dielectric surface as well as the penetration depth of the H^+:H_2^+ ions, we recommend bombarding the surface of the dielectric with N^+ ions. This could result in the formation of certain nitride complexes on the surface, which in turn could prevent the hydrogen ions from reacting with the dielectric surface molecules, thus eliminating the formation of the detrimental complexes on the surface.

5.2 : Conclusions for H^+:H_2^+ Implantation Study of a-Si:H Thin Film

H^+:H_2^+ bombardment of a-Si:H film can be used to re-introduce hydrogen into the film, especially to replace H which has diffused out of the film from the low density interstitial regions of columnar microstructures. Such implantation to a certain degree can be used to passivate electrical defects due to the removal of hydrogen and oxidation. However, ion implantation also generates defects in the surface through bond breaking, blistering and distortion. Annealing treatments of these surface defects might be possible. Since ion implantation induces defects on the surface, these could result in an increase of current leakage in the case of photovoltaic cells. For films of a few μm in thickness, ion energies of less than 30 keV are recommended. The intensity of the ion beam should also be adjusted so that the temperature of the target film remains in the vicinity of room temperature.

Figure 5.1 shows the surface of an a-Si:H film implanted with a 100 keV $H^+:H_2^+$ ion beam of 0.8 cm^2 area and a beam current of 76 μA. Since this is without a LN_2 cold trap in the target area, damage due to overheating is severe and is observable with the naked eye. Having set the upper limit of 30 keV for a-Si:H thin films, the optimum energies can only be chosen according to the structure (e.g. the size of columnar morphology and the respective degree of coalescence) and physical (e.g. density, thickness etc.) properties of the films themselves. In order to achieve a definite result from hydrogen ion implantation, beams of lower energy and intensity should be used. A cold trap should also be used in the target area to prevent contamination.

The four-point probe in this study is a useful facility. It yields anomalous conduction measuremens, but it does not destroy the films like the electrode deposition method. Since each a-Si:H film has its distinct characteristics, it is important that any indication of property change should be monitored in exactly the same spot of the film throughout the experiment. The four point probe in this study does just that.

5.3 : Conclusions of Plasma Interaction and Ion Implantation

The Raman data as obtained from the $H^+:H_2^+$ bombarded surface of a TiC wafer have been successfully utilized to confirm CH activity and methane formation and adsorption on the TiC (PS) surface. On the other hand, the titanium hydride formation for energies other than the 60 keV of the $H^+:H_2^+$ used is not confirmed. The effect of the energy vs. fluence of the hydrogen ions on the formation of

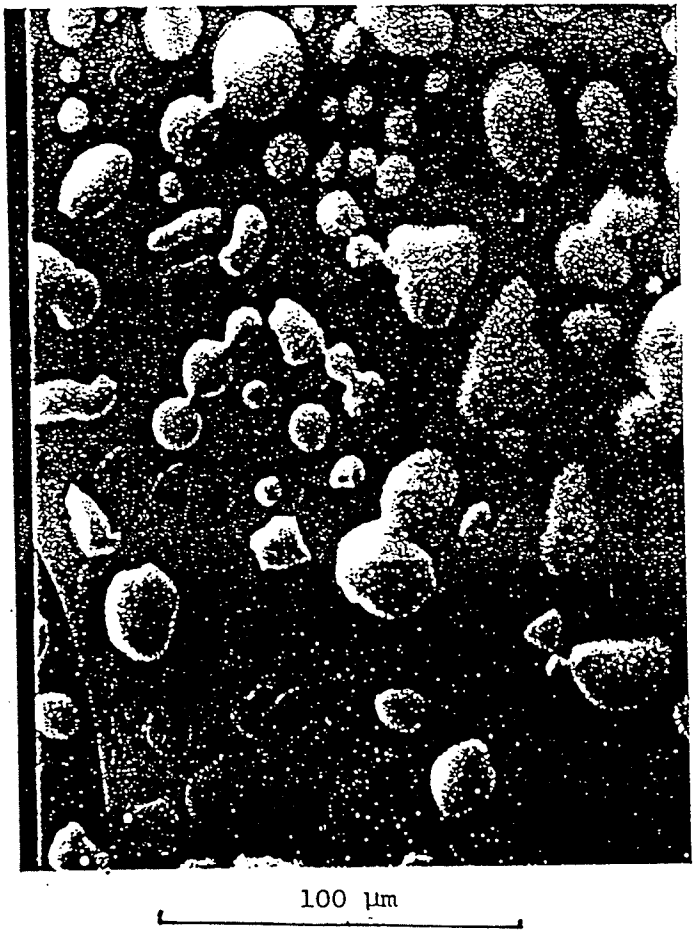

Figure 5.1 : Scanning Electron Micrograph (100x) shows total damage to the film after 100 keV hydrogen ion implantation. Bright spots are from the substrate.

carbon-hydrogen and titanium-hydrogen complexes is currently under investigation. The presence of carbon-hydrogen and titanium-hydrogen complexes on the surface of irradiated TiC(PS) coatings suggests the formation and absorption of various complexes of carbon-hydrogen and titanium-hydrogen. The out-diffusion of these complexes may be the reason for the amorphicity as observed by Fournier et al (50). They suggest that the amorphization starts when induced diffusion makes H concentrate around small grain boundaries and initiates the ionization process. We are suggesting that the concentration of hydrogen ions (from the plasma), and their build up on the surface, together with induced diffusion, can result in the formation of molecular complexes which can then be absorbed on the TiC surface. The out-diffusion of these complexes can poison the plasma as well as create low mobility vacancies and interstitials. This could result in inertial amorphization of the TiC surface.

KWOK CHUN-BUN
P. O. Box 1902
Winnipeg MB
R3C 3R2
Office (204) 474-6209, Home 269-9547

PUBLICATION

Quality Papers

1. C. B. Kwok, M. S. Mathur and J. S. C. McKee Energetic H_2^+ and D_2^+ Implantation of TiC in Simulation of Plasma Diffusion From a Thermonuclear Reactor CNA/CNS Student Conference 1989 in Winnipeg, ed. J. Mayer ISBN 1-895035-0-7, pp 111-116

2. J. J. G. Durocher, D. M. Gallop, C. B. Kwok, M. S. Mathur, J. K. Mayer, J. S. C. McKee, A. Mirzai, G. R. Smith and Y. H. Yeo A Search for Exidence of Cold Fusion in Direct Implantation of Palladium and Indium with Decterium 1989, Cdn. J. Phys. **V 67** pp 624-631, July 1989.

3. C. B. Kwok, M. S. Mathur and J. S. C. McKee C-H Activity of a TiC surface Implanted with H_2^+ J. of Nucl. Mat. **V 169** 1989.

4. M. S. Mathur, C. B. Kwok and J. S. C. McKee Energetic H_2^+ assisted Deposition of Thin Films of Ag and Au 1989, J. Phys. D: Appl. Phys. **V 22** pp 1228-1230, 1989 .

5. M. S. Mathur, C. B. Kwok and J. S. C. McKee Detection of Silver in Silicon J. Nucl. Inst. & Meth. in Phys. (Submitted) 1990.

6. C. B. Kwok, M. S. Mathur and J. S. C. McKee Plasma Interaction and Implantation Study of Refractory Material CNA/CNS Student Conference 1990 Trent University, Peterborough, Ont. ed. J. Jury, (to be Publish.)

Conference Papers / Abstracts

1. C. B. Kwok, M. S. Mathur and J. S. C. McKee High Energy Simulation of Aging and Environmental Effects on Dielectric Surfaces. CAP Conference Geulph Ontario, 1989. Physics in Canada **V. 45**, No. 3 pp 41

2. J. S. C. McKee, M. S. Mathur, G. R. Smith, C. B. Kwok, J. K. Mayer and Y. H. Yeo Report on Cold Fusion Experiment APS Spring Meeting 1989. Baltimore, U.S.A.

KWOK CHUN-BUN
P. O. Box 1902
Winnipeg MB
R3C 3R2
Office (204) 474-6209, Home 269-9547

3. M. S. Mathur, C. B. Kwok and J. S. C. McKee Energetic H_2^+ assisted Deposition of Thin Films of Ag and Au Proceedings: 16th International Conference on Metallurgical Coatings, San Diego, California 1989.

4. C. B. Kwok, M. S. Mathur and J. S. C. McKee Photoconductivity Improvement in H^+ implanted a-Si:H Thin Film. CAC - V Conference Proceedings, Montreal, Quebec 1988.

5. M.S. Mathur J.S.C. McKee and C.B. Kwok Molecular Complexes on Implanted Surfaces : Unenhanced Surface Raman Scattering Study. **VIII** International Conference on Ion Implantation Technology, 30th July - 3rd Aug 1990, University of Surrey, Guildford, United Kingdon.

6. Seven Quartary, One Annual Reports to Manitoba Hydro Since Sept. 1988

REFERENCES

1. J. Vermeer, Physica, **22**, 1269 (1956).
2. J.C. Anderson, Dielectrics, Chapman and Hall, London 1963.
3. J.J. O'Dwyer, The Theory of Dielectric Breakdown of Solids, Charandon Press, Oxford, 1964.
4. I. Bunget and M. Popescu, Physics of Solid Dielectrics, Elsevier, New York, 1984.
5. J.I. Pankove, Tetrahedrally-Bonded Amorphous Semiconductors, New York, Plenum p. 177, 1985.
6. Ibid W. Beyerp, p 129.
7. Ibid S. Guha, p 233.
8. Ibid M. Zavetova, I.P. Akimchenko, p157.
9. B. von Roerdern, L. ley and M. Cardona, Phys. Rev. Lett. **39**, p 1576 (1977).
10. V.A. Singh, C. Weigel, J.W. Corbett and L.M. Reth, Phys. Status Solidi, **B88**, p 637 (1977).
11. S.T. Picraus and F.L. Vook, Phys. Rev., **B18**, p 2066, (1978).
12. W. Primark and J. Luthra, J. Appl. Phys., **37**, p 2287 (1966).
13. G.S. Cargill, Phys. Rev. Lett., **28**, p 1372 (1972).
14. M.R. Havens, K.G. Mayhan, W.J. James and P. Schmidt, J. Appl. Polym. Sci, **22**, p 2793 (1978).
15. Ibid. p 2799.
16. J.C. Knights J. Non-Cryst. Solid., **36), p 159 (1980).**

17. S.R. Meija, R.D. Mcleod, K.C. Kao and H.C. Card, Rev. Sci. Instrum., **57** (3) 1986.

18. R.S. Nowicki, W.D. Buckley, W.D. Mackintosh and I.V. Mitchell, J. Vac. Sci. Technol., **11**, p 675, 1974.

19. A.G. Dirks and H.J. Leamy, Thin Solid Films, **47**, p 219 (1977).

20. C. Brunet, S. Dallaire and R.G. Saint-Jacques, J. Vac. Sci. Technol. **A3**, 2503 (1985).

21. M.S. Mathur, V.P. Derenchuk and J.S.C. McKee Cnd. J. Phys., v62 N3 (1984).

22. M.S. Mathur C.B. Kwok and J.S.C. McKee Energetic H^+:H_2^+ Assisted Deposition of Thin Films of Ag and Au, accepted by **J. Phys. D: Applied Physics** (1989),

23. K.H. Arunkumar, H.A. Marzouk and E.B. Bradley, Rev. Sc. Int. (1984).

24. J.S.C. McKee, C.P. Randell and S.F.J. Wilk J. Phys. D: Appl. Phys. **9** L159 1976.

25. Y. Gomay, K. Kawahata, N. Noda, and S. Tanahashi, J. Nucl. Mater. 111/112, **323** (1982).

26. Discussion Farady Society **9**, 92, 1950.

27. Hirschmann, Kriseley and Fassel, Spect. Chem. **21**, 2125 (1965).

28. J.R. Schever, Spect. Chem. Acta, **24A**, 747 (1968).

29. G. Herzberg, D. Van Nostrand, Infrared and Raman Spectra, 1968.

30. R.G. Dickenson, R.T. Dillon and F. Rasetti, Phys. Rev. **34** (1929) 582.

31. G.E. MacWood and H.C. Uuey, J. Chem. Phys. **4** (1936) 402.

32. D.M. Dennison, Rev. Mod. Phys. **12** (1940) 175.

33. G. Glockfer and C.E. Morrell, J. Chem. Phys. 4, 15 (1936).

34. G. Herzberg, Infrared and Raman Spectra, D. Van Nostrand Co. (1968).

35. H. Kaesz and Saillant, Chem. Rev. **72**, 231 (1972).

36. W. Ho, N.J. DiNardo and E.W. Plummer, J.Vac. Sci. Technol. **17**, 134 (1980).

37. N.E.W. Hartley, Surface Treatment for Protection, **3** (10) Inst. Metall, London, pp 197-209.

38. N.E.W. Hartley, G. Dearnaley, T.F. Turner and J. Saunders, in Applications of Ion Beams to Metals, eds. Picraux, E.P. EerNisse and F.L. Vosk, Plenum, New York pp 123-138, 1974.

39. D.H. Jack and K.H. Jack, Mater. Sci. Eng., 11, pp 1-27 (1973).

40. N.E.W. Hartley, Tribology, 8, pp 65-72 (1975).

41. N.E.W. Hartley, Inst. Phys. Conf. Sci., **28**, pp 210-223 (1976).

42. S.E. Harding M.Sc. Thesis. Brighton Polytechnic (1977).

43. J.K. Hirvonen, J.W. Butter, T.P. Smith, R.A. Kent and V.C. Westcott, Radiat. Eff. (Submitted for publication 1978, quoted in Hirovonen 1978).

44. G. Longworth and N.E.W. Hartley, Thin Solid Films, **48**, pp 95-104 (1978).

45. W.W. Hu, C.R. Clayton, H. Herman and J.K. Hirvonen, Sci. Met., **12**, pp 697-698 (1978).

46. W.W. Hu, C.R. Clayton, H. Herman and J.K. Hirvonen, Ion Implantation Metallurgy, eds. L.M. Preece and J.K. Hirvonen, TMS-AME, New York 1980.

47. M.S. Mathur, V.P. Derenchuk and J.S.C. McKee, Can. J. Phys., **62**, 214 (1984).

48. C.J. Dienes and G.H. Vineyard, Radiation Effects in Solids, Wiley (interscience), New York 1957.

49. M.W. Thompson, Defects and Radiation Damage in Metals, Cambridge Univ. Press, London and New York 1969.

50. D. Fournier, M.O. Ruault and R.G. Saint-Jacques, Nucl. Inst. and Methods in Phys. Research **B**19/20, 559 (1987).